Journal Pre-proof

Water-Soluble Inhibitors of ABCG2 (BCRP) – A Fragment-Based and Computational Approach

Frauke Antoni, David Wifling, Günther Bernhardt

PII: S0223-5234(20)30930-2

DOI: https://doi.org/10.1016/j.ejmech.2020.112958

Reference: EJMECH 112958

To appear in: *European Journal of Medicinal Chemistry*

Received Date: 29 April 2020

Revised Date: 16 October 2020

Accepted Date: 18 October 2020

Please cite this article as: F. Antoni, D. Wifling, G. Bernhardt, Water-Soluble Inhibitors of ABCG2 (BCRP) – A Fragment-Based and Computational Approach *European Journal of Medicinal Chemistry*, https://doi.org/10.1016/j.ejmech.2020.112958.

low water solubility
(< 100 nM)

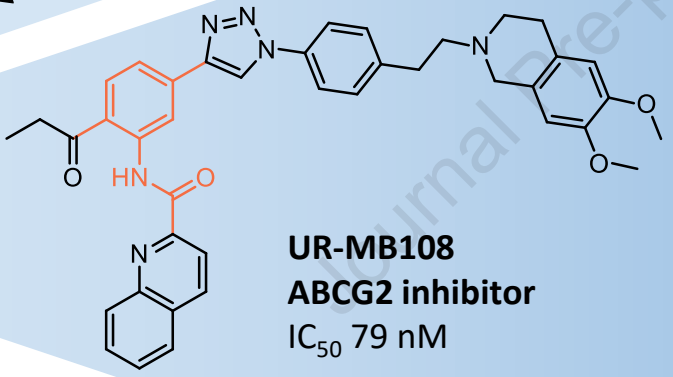

UR-MB108
ABCG2 inhibitor
IC_{50} 79 nM

high water solubility
(≥ 1 µM)

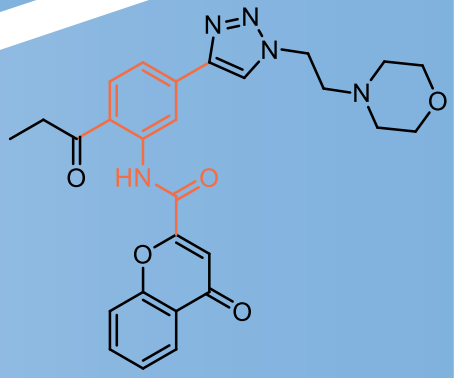

UR-Ant116
triple ABCG2/B1/C1 inhibitor
IC_{50} 312 nM/ 1.3 µM/ 2.1 µM

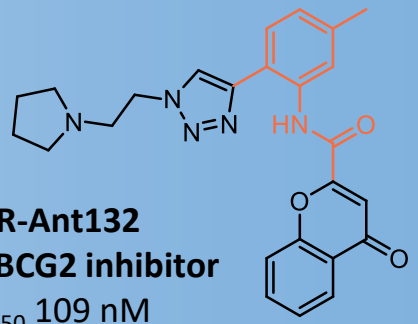

UR-Ant132
ABCG2 inhibitor
IC_{50} 109 nM

Water-Soluble Inhibitors of ABCG2 (BCRP) – A Fragment-Based and Computational Approach

Frauke Antoni*, David Wifling[#], Günther Bernhardt

Institute of Pharmacy, University of Regensburg, D-93040 Regensburg, Germany

Abstract

A good balance between hydrophilicity and lipophilicity is a prerequisite for all bioactive compounds. If the hydrophilicity of a compound is low, its solubility in water will be meager. Many drug development failures have been attributed to poor aqueous solubility. ABCG2 inhibitors are especially prone to be insoluble since they have to address the extremely large and hydrophobic multidrug binding site in ABCG2. For instance, our previous, tariquidar-related ABCG2 inhibitor UR-MB108 (**1**) showed high potency (79 nM), but very low aqueous solubility (78 nM). To discover novel potent ABCG2 inhibitors with improved solubility we pursued a fragment-based approach. Substructures of **1** were optimized and the fragments 'enlarged' to obtain inhibitors, supported by molecular docking studies. Synthesis was achieved, i.a., via Sonogashira coupling, click chemistry and amide coupling. A kinetic solubility assay revealed that **1** and most novel inhibitors did not precipitate during the short time period of the applied biological assays. The solubility of the compounds in aqueous media at equilibrium was investigated in a thermodynamic solubility assay, where UR-Ant116 (**40**), UR-Ant121 (**41**), UR-Ant131 (**48**) and UR-Ant132 (**49**) excelled with solubilities between 1 µM and 1.5 µM – an up to 19-fold improvement compared to **1**. Moreover, these novel *N*-phenyl-chromone-2-carboxamides inhibited ABCG2 in a Hoechst 33342 transport assay with potencies in the low three-digit nanomolar range, reversed MDR in cancer cells, were non-toxic and proved stable in blood plasma. All properties make them attractive candidates for in vitro assays requiring long-term incubation and in vivo studies, both needing sufficient solubility at equilibrium. **41** and **49** were highly ABCG2-selective, a precondition for developing PET tracers. The triple ABCB1/C1/G2 inhibitor **40** qualifies for potential therapeutic applications, given the concerted role of the three transporter subtypes at many tissue barriers, e.g. the BBB.

Keywords

ABCG2 transporter, BCRP, Inhibitors, Hoechst 33342, Water solubility, Rule of five

1 Introduction

Water solubility of a compound is indispensable for its biological activity: undissolved, a molecule cannot reach its target. This is a simple fact, however often undervalued. There is a general tendency in drug discovery towards large and lipophilic molecules – such compounds are more likely to be identified as 'hits' in high-throughput screenings (in which the compounds are added 'pre-dissolved' in DMSO) [1,2], and during the optimization of the 'hits' often additional lipophilic substituents are attached [3]. The dilemma is that higher lipophilicity is strongly connected with increased in vitro activity [2,4], because hydrophobic interactions are the dominant driving forces in small-molecule ligand-protein binding processes [5,6]. Frequently, drug discovery strategies lead to a substance with high activity and selectivity but very poor aqueous solubility [1,2].

This phenomenon causes immense problems, because aqueous solubility plays an essential role in virtually every phase of the discovery and development of pharmacological tools and drugs [3,7]. It already begins in the purification process, where RP-HPLC is commonly the method of choice, for which the substance needs to be dissolved in a water-containing eluent. In biological in vitro studies, low solubility leads to erratic and erroneous assay results [3]. If precipitation occurs before the compound can reach its target, the actual concentration is lower than intended and the substance appears less active [3,8]. Hence, structure-activity relationship analyses are compromised [9] and off-target activities may become undetectable [3]. In vivo, after oral administration, poor water solubility results in inadequate resorption [1-3,8,10]. Self-evidently, the compound needs to be dissolved in the aqueous gastrointestinal fluids in order to cross the intestinal membranes, and the flux (passive diffusion) is directly proportional to the concentration gradient of the agent between the intestinal lumen and the blood [1]. Poorly soluble compounds are particularly susceptible to food effects (on drug absorption) and often special excipients are required, which can impair the results of in vivo studies [3]. Not only oral drug forms, but also parenteral formulations depend heavily on sufficient aqueous solubility, water being the solvent of choice for intravenous administration [10]. Furthermore, in organisms, poorly soluble drugs may precipitate at high concentrations and cause adverse effects such as phlebitis [11]. Taken together, sufficient aqueous solubility is of major importance for both drugs and pharmacological tools and low solubility of drug candidates has been the cause of numerous failures in drug development [12].

When addressing solubility problems, formulation technology can help, but this approach is expensive and there is no guarantee of success [1-3,9]. Therefore, the primary strategy should be to improve solubility by adequate alterations of the chemical structure of the molecule [2,9,13]. Such structural changes fall into three categories: they aim either at (I) decreasing the crystal packing energy, e.g. by disrupting planarity, [2,7,13-15] (II) increasing the solvation energy, for example by attaching polar or ionizable groups [2,7,13,15] or at (III) reducing the cavitation energy [16] – required to form a cavity in the water structure in order to host the solute molecule, which results in a concomitant decrease in entropy – for instance by reducing the size of the molecule [2,15]. Whether these structural changes actually enhance the solubility is hard to predict, also when in silico methods are applied [2]. In 1997, Lipinski et al. published their seminal article on the well-known 'rule of five' (Ro5) [1]. Using a library of drugs with 'good' resorption properties (i.e. drugs that passed clinical Phase II selection), the group identified four calculable parameters to estimate resorption by free diffusion, a process which is dependent on sufficient solubility and permeability. The authors concluded that resorption problems are more likely to occur, when there are more than five H-bond donors, ten H-bond acceptors, the molecular weight (MWT) is higher than 500 Da and the calculated logP (clogP) is higher than five (all values are five or multiples thereof) [1]. Since then, a couple of drugs that violate one or more Ro5 – Ro5-outliers – have emerged (e.g. the anticancer drug Navitoclax [17]), but the bottom line of articles on the subject is mostly the same: the development of 'beyond-Ro5' drugs is feasible and for some targets necessary, but extremely difficult, and there is a high probability of failure [18-20]. Therefore, medicinal chemists are well-advised to take the Ro5 into consideration when designing novel chemical entities.

Ultimately, with the designed compound in hand, solubility can be assessed experimentally to find out if the solubility-optimization process was successful. Usually a distinction is made between the kinetic and the thermodynamic (equilibrium) solubility of a compound (c.f. section 2.4). What levels of equilibrium solubility are required for pharmacological tools and drugs is debated, but a range between 1 µM to 0.1 M may be considered as a drug solubility window [21]. As a rule of thumb, the solubility of a compound should be at least three times its IC_{50} value [22].

The target we address in this study – ABCG2 – is a member of the ATP-binding cassette (ABC) transporter superfamily [23]. It functions as an exporter and is predominantly expressed in the plasma membrane [24]. Inhibitors of ABCG2 have been developed as pharmacological tools to study the patho(physiological) role of this transporter and as a means

to overcome the blood-brain barrier (BBB) [25] or multidrug resistance (MDR) in cancer [26]. During the development of ABCG2 inhibitors the focus has been on optimizing their potency and selectivity. In a few cases [27,28], efforts have been made to improve some of their drug-like (i.e. ADME-Tox) properties, mainly to increase their stability or decrease their toxicity. But their physicochemical properties, especially their water solubility, have been neglected so far. Aqueous solubility has not been a parameter much taken into consideration and up to now no solubility-driven optimization of ABCG2 inhibitors has been reported. The outcome is that most ABCG2 inhibitors described so far are relatively large and lipophilic molecules. Increasing the aqueous solubility of ABCG2 inhibitors is a great challenge, because ABCG2, much more than many other targets, requires ligands that show high lipophilicity and size. In contrast to ligands of membrane-spanning receptors, an ABCG2 inhibitor must permeate through the cell membrane to reach its target, i.e. the multidrug binding site, which was recently identified by cryo-EM studies [29,30]. Moreover, as revealed in the aforementioned structural studies, the binding site is comparatively large and markedly hydrophobic.

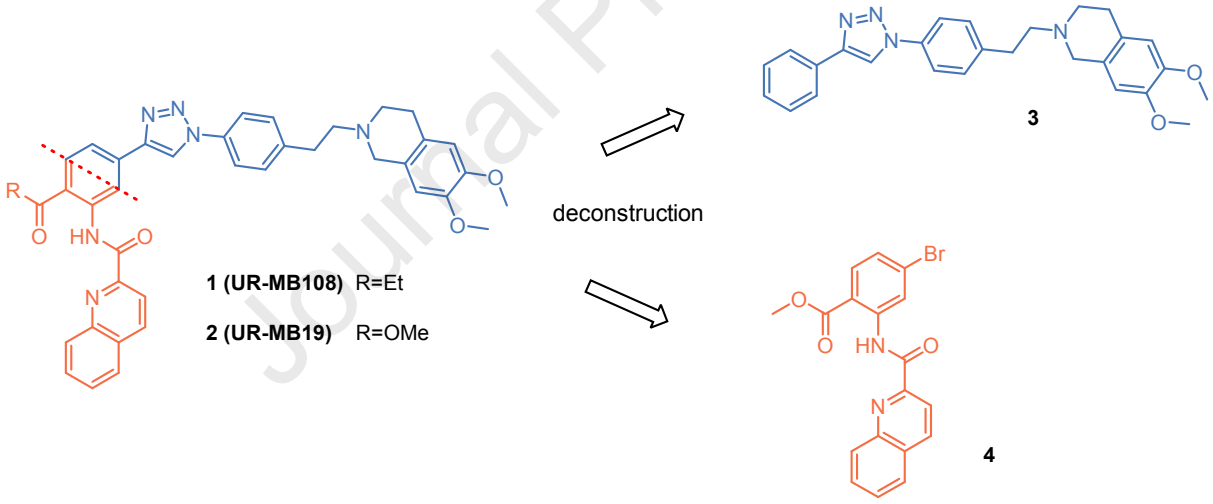

Figure 1. Our previous tariquidar-related ABCG2 inhibitors UR-MB108 (**1**) and UR-MB19 (**2**) and rationale of our fragment-based approach: deconstruction of **2** to the fragments **3** and **4**.

Previously we reported on tariquidar-related triazoles (such as UR-MB108 (**1**); **Figure 1**) as selective and stable inhibitors of ABCG2 [28]. Inhibitor **1** acted as a potent and effective ABCG2 transport and ATPase inhibitor. Accordingly, it appeared to stay in solution at least for the short time span of the transport and ATPase assay. Unfortunately – preempting one result of the present study – the equilibrium solubility of inhibitor **1** was as low as 78 nM, neither reaching the level of at least 1 µM mentioned above, nor fulfilling the rule of thumb, the IC_{50} value of **1** also being around 80 nM. In the present study, we set out to design and prepare potent and stable ABCG2 inhibitors with improved equilibrium water solubility,

using our previous inhibitors (**1** and UR-MB19 (**2**); **Figure 1**) as a starting point. To this end, we pursued a fragment-based approach, which we considered suitable for our predicament because of the following reasons: high-affinity ligands that are small have been shown to bind with favorable enthalpy, dominated by optimal polar interactions [31,32], whereas for larger ligands entropy changes become increasingly important (coming mainly from the desolvation; water molecules from the solvation shell are released and join bulk water) [31,32]. Therefore, ligands optimized in a fragment-based approach are more likely to be relatively low in hydrophobicity and small in size [31,32]. Moreover, fragments are easier to prepare synthetically, so this strategy is also time-saving. **Figure 1** shows the rationale of our fragment-based approach: compound **2** was 'deconstructed' to the fragments **3** and **4** for analysis and optimization. When 'enlarging' the new fragments to obtain potent and soluble inhibitors, we took advantage of the recently published cryo-EM structure of ABCG2 in complex with inhibitors [29], too, and used molecular docking studies to optimize protein-ligand interactions. In addition, we considered Lipinski's Ro5 when designing our novel inhibitors. Furthermore, we established thermodynamic and kinetic solubility assays suitable for analyzing compounds in the comparatively low solubility range of ABCG2 inhibitors.

2 Results and Discussion

2.1 Design and Synthesis

We designed fragment **4** in a way that it contains a more readily accessible ester moiety (like in **2**), instead of a more stable ketone function (as in **1**), because stability was not an issue in case of the fragments; they merely served as a starting point for structural optimizations and 'enlarging' or merging/linking with other fragments to obtain potent inhibitors [33]. The introduction of a ketone group only gave very low yields, whereas the building block comprising the ester was commercially available.

The synthesis of the fragments **3** and **4** is shown in **Scheme 1**. Compound **3** was prepared in a copper-catalyzed azide-alkyne cycloaddition (CuAAC), belonging to a set of synthetic procedures termed 'click' reactions due to their convenience, versatility and achievement of high yields [34]. The azide for the 'click' reaction was synthesized according to our previous report [28]. 1-(2-bromoethyl)-4-nitrobenzene (**5**) was treated with 6,7-dimethoxy-1,2,3,4-tetrahydroisoquinoline (**6**) in an N-alkylation reaction to give compound **7**, then the nitro group was hydrogenated to an amine group (yielding **8**) and converted to an azide, resulting in compound **9**, which was introduced into a 'click' reaction with phenylacetylene (**10**). In this variant of the CuAAC we used the polytriazole TBTA as a copper(I)-stabilizing ligand.

Fragment **4** was synthesized by amide bond formation from methyl 2-amino-4-bromobenzoate (**11**) and quinoline-2-carboxylic acid, using TBTU as a coupling reagent. Compound **11** is a building block of our previous inhibitor **2** and was therefore abundantly available in our laboratory. In pursuit of convenient, fast and economic procedures, we used **11** for synthesizing compound **4** (and further fragments), which is the reason for the presence of bromine in the respective substructure.

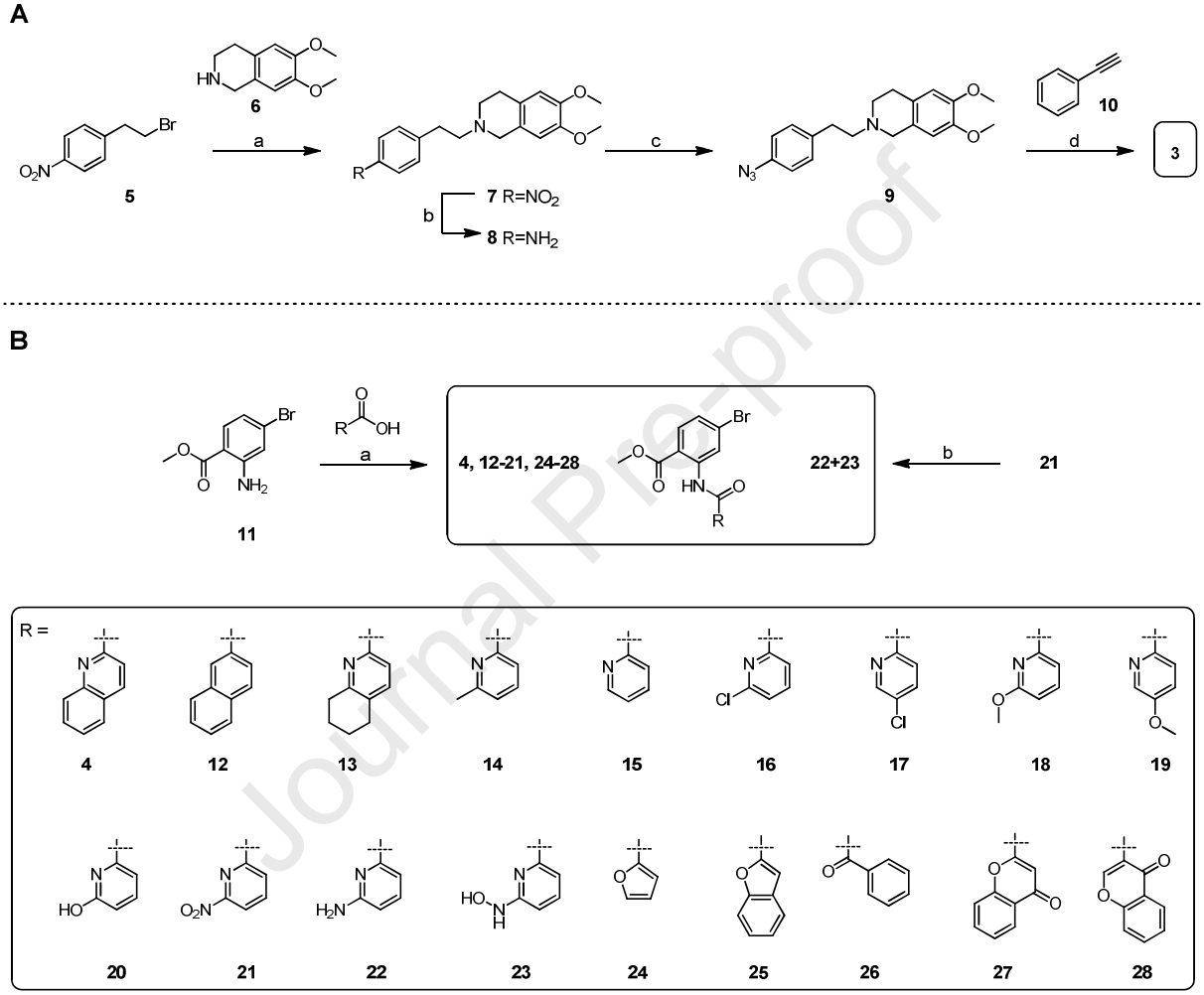

Scheme 1. (A) Synthesis of fragment **3**. Reagents and conditions: (a) K_2CO_3, MeCN, 130 °C (microwave), 70 min, 62%; (b) Pd/C, H_2 (10 bar), EtOH, rt, overnight, 71%; (c) (I) $NaNO_2$, 6 M HCl aq, 0 °C, 1 h; (II) NaN_3, 0 °C → rt, 2 h; 92%; (d) $CuSO_4$, sodium ascorbate, TBTA, $CHCl_3$, reflux, 1 d, 66%. **(B)** Synthesis of the fragments **4** and **12-28**. Reagents and conditions: (a) respective carboxylic acid, TBTU, DIPEA, DMF, 80 °C (microwave), 30 min; or respective carboxylic acid chloride (carboxylic acid, $SOCl_2$, pyridine, toluene, reflux, 2 h), DIPEA, DCM, 0 °C, overnight; 3-78%; (b) $HSiCl_3$, DIPEA, DCM, 0 °C → rt, overnight, 13-30%.

Based on the inhibitory potency and efficacy of the two fragments **3** and **4**, fragment **4** was selected for further optimization and study. We replaced the quinoline moiety by 17 different groups, yielding the novel fragments **12-28** (**Scheme 1B**). Our strategy for designing the fragment library derived from compound **4** was as follows: we performed structural changes aiming at improved solubility and/or we introduced substructures known to confer inhibitory potency at ABCG2. In order to gain structural information, we performed an X-ray analysis of

a crystal of **4** (**Figure 2**). This showed that the molecule was present in a flat conformation and that there was a hydrogen bond between the ester carbonyl oxygen and the amide hydrogen. The quinoline nitrogen faced the amide hydrogen, probably due to dipole-dipole interaction. As a trend, the higher the planarity the more π-π stacking is possible, contributing to crystal lattice stability [4]. The solubility can be increased by disrupting planarity, thus decreasing the crystal lattice energy. We implemented this idea by substituting the quinoline nitrogen by a carbon (**12**) (in the hope of decreasing the dipole-dipole interactions with the amide hydrogen, thereby allowing rotation), by increasing the fraction of sp^3-hybridized carbon (**13**, **14**) and by omitting one aromatic ring (**15**). Destabilizing the crystal lattice is a useful approach, when high lipophilicity is required by targets such as ABCG2. We also made efforts to decrease the logP value by introducing polar groups (substituting one aromatic ring) (**16**-**23**) or by substituting the quinoline nitrogen by oxygen (more electronegative), hence increasing polarity (**24**-**26**). Fragments **18** and **19** bear methoxy groups, which are present in many known ABCG2 inhibitors [35-39], and compound **21** contains a nitro group, also found in a number of ABCG2 inhibitors [40,41]. Furthermore, chromone is a very prominent substructure of numerous ABCG2 inhibitors reported [42-44] and is a structural element of the fragments **27** and **28**.

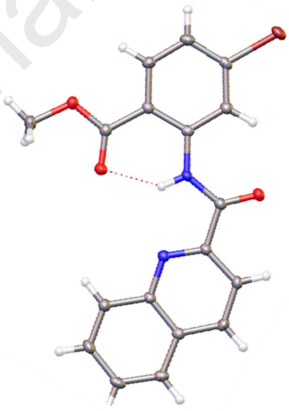

Figure 2. Structure of compound **4**, determined by X-ray analysis.

Like their precursor **4**, the fragments **12**-**21** and **24**-**28** were synthesized from **11** and the respective carboxylic acid by amide bond formation (**Scheme 1B**). The carboxylic acids employed were all commercially available, except the corresponding acid for fragment **13**. The acid was synthesized according to literature [45]. 5,6,7,8-Tetrahydroquinoline was oxidized at the nitrogen with 3-chlorobenzoperoxoic acid, yielding 5,6,7,8-tetrahydroquinoline 1-oxide (**29**), then treated with trimethylsilyl cyanide and dimethylcarbamoyl chloride to form 5,6,7,8-tetrahydroquinoline-2-carbonitrile (**30**) and afterwards hydrolyzed with hydrochloric acid to 5,6,7,8-tetrahydroquinoline-2-carboxylic acid (**31**). The fragments **22** and **23** were obtained by

reduction of the nitro group in compound **21** to an amino group (in **22**) and a hydroxyl amino group (in **23**), using trichlorosilane.

According to the biological results of the novel fragments, we chose compound **27**, containing a chromone moiety, for further optimization and 'decorating', yielding a chromone-based series of inhibitors (comprising two subsets; **Scheme 2**) Aiming at increased solubility, we introduced solubilizing groups such as basic, acidic and hydroxyl moieties.

In a first chromone subset, we introduced solubilizing groups via 'click' chemistry in meta-position to the amide moiety (replacing the bromine), analogous to our previous inhibitors **1** and **2**, which bear a triazole ring in an equivalent position. For this purpose, we converted protonatable 2-morpholinoethyl chloride (**32**) and 2-pyrrolidoethyl chloride (**33**) into the corresponding azides (**34** and **35**) (**Scheme 2A**). Besides, we employed the azide **9** and commercially available azides containing a hydroxyl group or a carboxylic acid. For stability reasons, we also substituted the ester moiety by a ketone. The latter was synthesized by acylating 3-ethynylaniline (**36**) in ortho-position to the amine group in a variant of the Sugasawa reaction, using $GaCl_3$ as a Lewis acid (forming **37**). Then the chromone-2-carboxylic acid was introduced by amide bond formation, giving compound **38**, which was treated with the respective azide in a 'click' reaction to form the inhibitors **39**-**43** (**Scheme 2B**).

We performed molecular docking experiments with fragment **27**, using the recently published cryo-EM structure of ABCG2 in complex with inhibitors (see section 2.2). Based on these experiments, we created a second chromone subset, in which we introduced solubilizing groups (also via 'click') in ortho-position to the amide moiety, substituting the ester group, and a methyl group meta to the amide group (substituting the bromine). The synthesis started from 2-iodo-5-methylaniline (**44**), which was coupled with trimethylsilysacetylene in a Sonogashira reaction (yielding the alkyne **45**), deprotected with potassium carbonate to **46**, treated with chromone-2-carboxylic acid to form the amide **47** and then submitted to CuAAC with the respective azide, resulting in the inhibitors **48**-**50** (**Scheme 2C**).

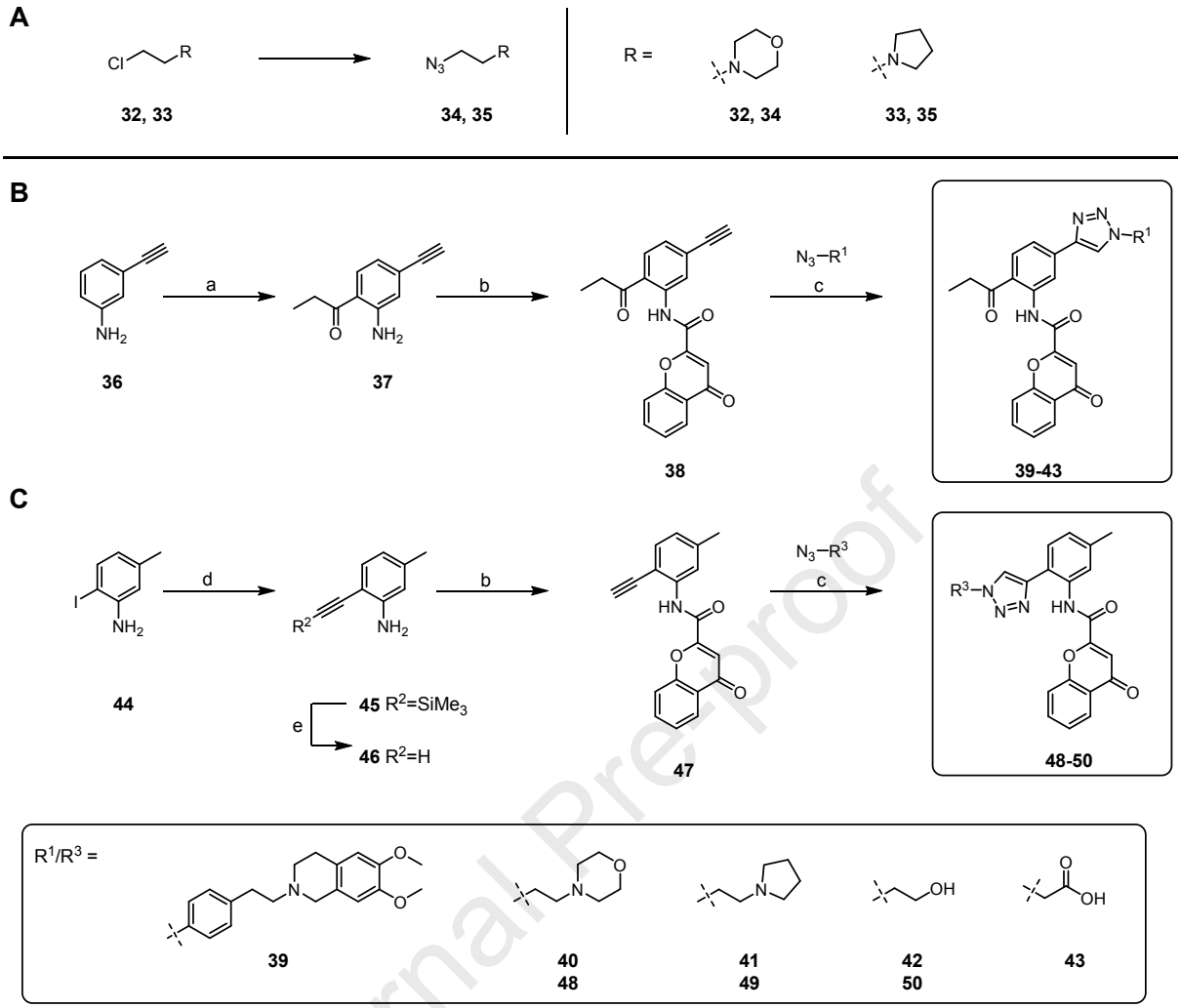

Scheme 2. (A) Synthesis of the azide building blocks **34** and **35**. Reagents and conditions: NaN_3, H_2O, 130 °C (microwave), 1 h, 21-29%. **(B+C)** Synthesis of the inhibitors **39**-**43** (B) and **48**-**50** (C), bearing a chromone moiety. Reagents and conditions: (a) (I) propionitrile, BCl_3, $CHCl_3$, 0 °C; (II) $GaCl_3$, 0 °C, 10 min → rt → reflux, overnight; (III) 2 M HCl aq, 0 °C → 70 °C, 2 h; 14%; (b) 4-oxo-4*H*-chromene-2-carboxylic acid, TBTU, DIPEA, DMF, 80 °C (microwave), 30 min, 30-57%; (c) respective azide, $CuSO_4$, sodium ascorbate, TBTA, $CHCl_3$, reflux, 2-3 d, 14-84%; (d) trimethylsilylacetylene, $Pd(PPh_3)_2Cl_2$, CuI, NEt_3, THF, rt, 90 min, 91%; (e) K_2CO_3, MeOH, rt, 2 h, 75%.

In addition to the compounds derived from fragment **27**, we prepared a second series (**Scheme 3**), in which we merged fragments showing activity similar to their precursor **4**, with fragment **3**. By analogy with our previous inhibitor **1**, we also replaced the ester moiety by a ketone group in order to provide for chemical stability. This series was synthesized from compound **37**, which was treated with the corresponding carboxylic acids to form the amides **51**-**58** and then introduced into a 'click' reaction with the azide **9**, yielding the inhibitors **59**-**64**, **66** and **58**. Compound **65** could not be synthesized in this way – the CuAAC failed – so **65** was formed by treating **37** with **9** under 'click' conditions first (resulting in **69**) and then introducing the corresponding carboxylic acid to form the amide bond. By analogy with the corresponding fragment **22**, compound **67** was synthesized from **66** by reducing the nitro group with ammonium formate, using palladium on charcoal as a catalyst.

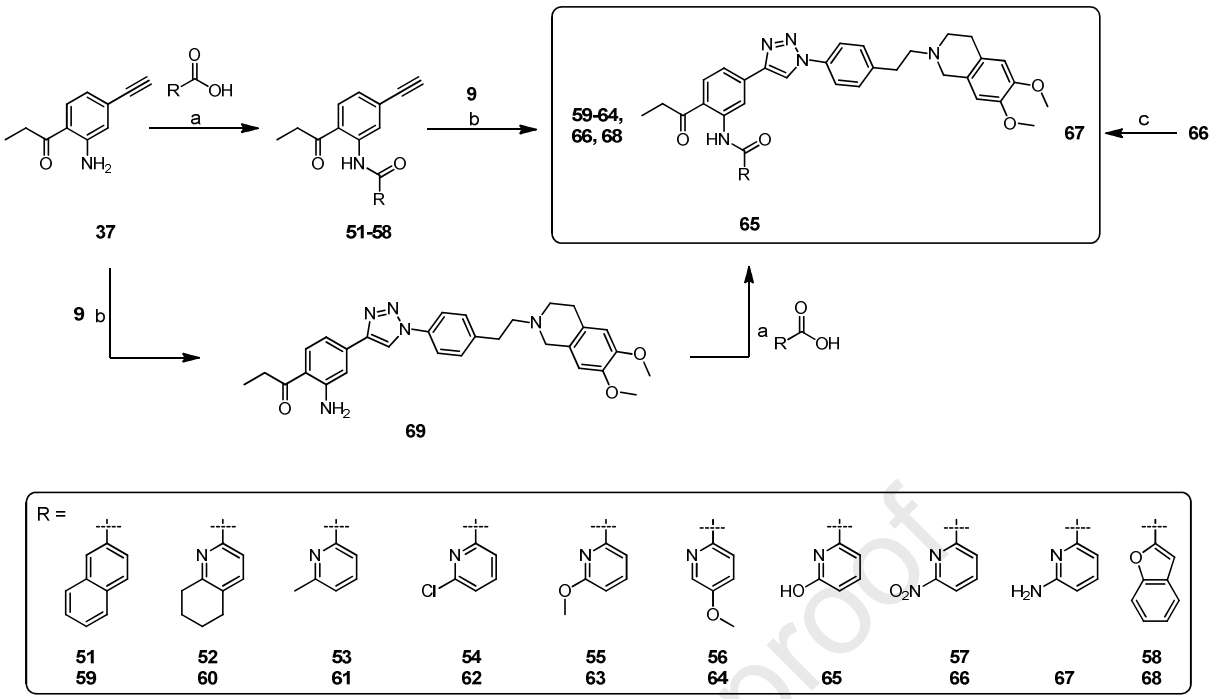

Scheme 3. Synthesis of the inhibitors **59**-**68**. Reagents and conditions: (a) corresponding carboxylic acid, TBTU, DIPEA, DMF, 80 °C (microwave), 30 min; or corresponding carboxylic acid chloride (carboxylic acid, $SOCl_2$, pyridine, toluene, reflux, 2 h), DIPEA, DCM, 0 °C, overnight; 5-86% (b) $CuSO_4$, sodium ascorbate, TBTA, $CHCl_3$ or THF or DMSO/2-propanol, reflux, 1-3 d, 12-53%; (c) ammonium formate, Pd/C, THF/MeOH, reflux, overnight, 52%.

2.2 Molecular Docking

We performed molecular (induced-fit) docking experiments with our most potent fragment **27** (see **Table 1**), using the recently reported cryo-EM structure of the ABCG2 transporter (PDB ID: 5NJ3 [30]). Based on our calculations, the most probable binding site is located between the two ABCG2 monomers in the center of the transmembrane domain (**Figure 3A**), which is in agreement with a cryo-EM structure of ABCG2 in complex with small molecule inhibitors [29]. Within this cavity, the carbonyl oxygen in the ester moiety of **27** formed a hydrogen bond with N436 of the first monomer, and the chromone ring structure established π-π contacts with the phenyl ring of F439 belonging to the second monomer (**Figure 3B**). Noteworthily, one molecule of compound **27** bound to both ABCG2 monomers and connected them with each other (as did our much larger previous inhibitor UR-MB136 in the cryo-EM structure [29]). In contrast, two molecules of MZ29, also rather a small inhibitor, proved [29] to bind to the ABCG2 transporter. Fragment **27** served as a starting point for structural optimization. Retaining the *N*-phenyl-chromone-2-carboxamide scaffold, we varied both, the nature and the position of the substituents at the central phenyl ring. Thereby we considered stability as well as solubility aspects, e.g. by substituting the labile ester moiety and introducing polar groups such as heterocycles and hydroxyl groups. Guided by a low XP Gscore, visual inspection of the binding poses and synthetic feasibility, we selected compound **48** (**Figure 3C**) for synthesis and characterization. Compounds **49** and **50** were

derived from **48**. Compound **48** seemed favorable because it showed interactions similar to those of **27**, which had already been proven very potent in the biological assays: there was a hydrogen bond between the triazole ring and N436 (first monomer) and π-π stacking between the chromone ring and the phenyl ring of F439 (second monomer). We chose a methyl group in para position to the triazole ring to optimally occupy the hydrophobic pocket formed by F431, F432 and two other residues not depicted in the figure (M549 and L555). The position of the triazole ring was chosen not only because of the favorable hydrogen bond, but also because the rather spacious morpholine ring, which is attached to the triazole ring via an ethylene linker, is directed towards the wide, intracellular part of the pore between the two ABCG2 monomers.

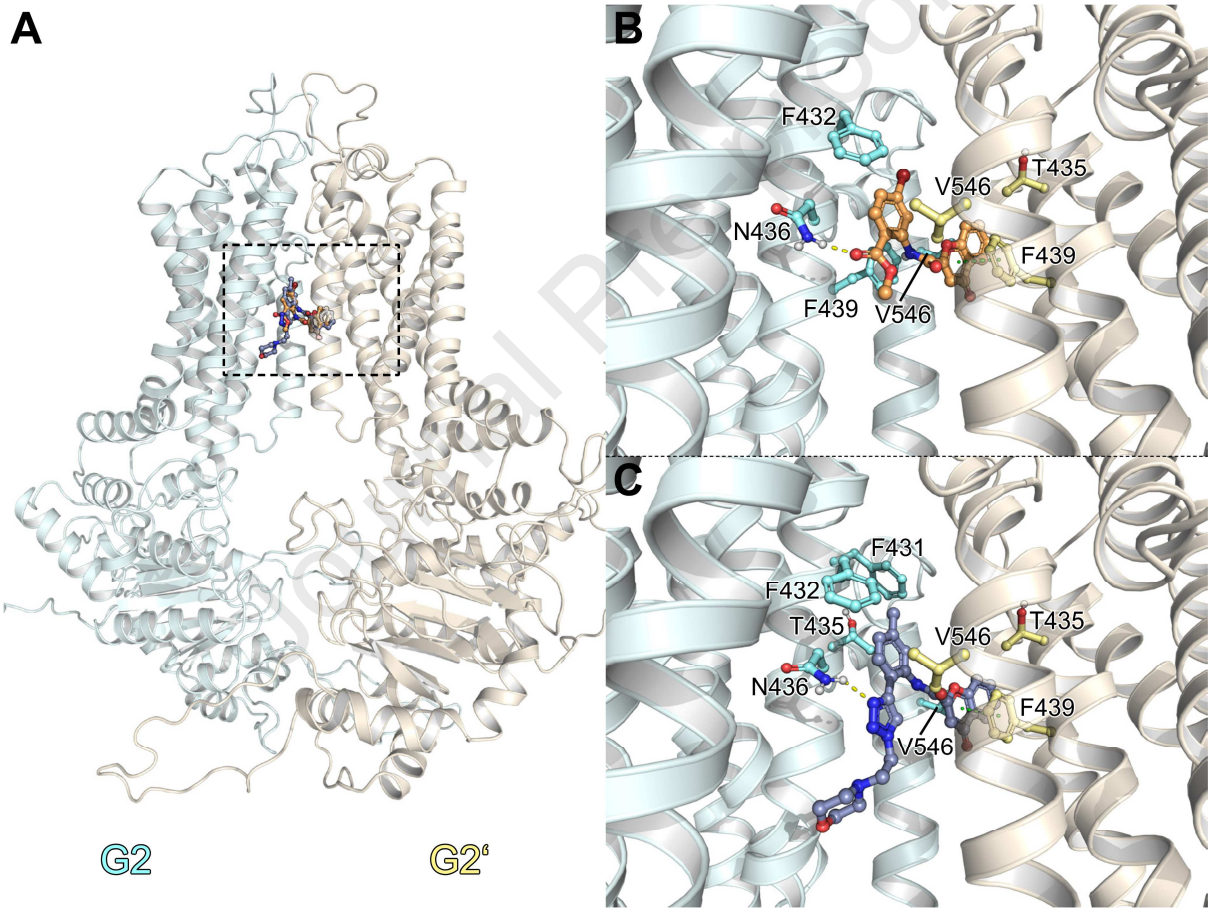

Figure 3. Binding poses of **27** and **48** obtained from induced-fit docking to the ABCG2 transporter. **(A)** Ribbon illustration of the ABCG2 homodimer, with individual G2 monomers colored blue and yellow. Bound ligand (**27** and **48**) molecules are colored orange and violet, respectively. **(B+C)** Specific interactions between **27** (B) or **48** (C) and ABCG2 residues within the binding pocket are highlighted: the respective residues are labelled, hydrogen bonds are indicated as yellow, and π-π stacking as green, dashed lines.

2.3 Biological Characterization

2.3.1 Inhibition of the ABCG2, ABCB1 and ABCC1 Transport Activity

In order to investigate an inhibition of ABCG2-mediated transport activity by our compounds, we performed a Hoechst 33342 microplate assay, using ABCG2-expressing MCF-7/Topo

cells. Hoechst 33342 is a substrate of ABCG2, which accumulates in the cells upon ABCG2 inhibition and can be detected fluorometrically (after DNA-intercalation). In addition, we analyzed the effect on the transport activity of ABCB1 and ABCC1 in a calcein-AM microplate assay, using KB-V1 and MDCK.2-MRP1 cells, respectively. By analogy with the Hoechst 33342 assay, the accumulation of the dual ABCB1/C1 substrate calcein-AM is determined by measuring the fluorescence after intracellular cleavage to calcein, which fluoresces in complex with Ca^{2+}-ions.

The fragments **3** and **4**, representing partial structures of our previous, tariquidar-related ABCG2 inhibitors (**1** and **2**), showed distinct behavior in the Hoechst 33342 assay. Whereas compound **3** was only 41% effective, fragment **4** was as effective as **1** and **2**, namely 86%, and showed a moderate IC_{50} value of 1.9 µM (**Figure 4A** and **Table 1**). Therefore, we considered **4** as a starting point for optimization. The novel fragments derived from **4** (compounds **12**-**28**), in which the quinoline moiety was replaced by other groups, were analyzed for inhibition of ABCG2, ABCB1 and ABCC1 at a concentration of 10 µM (**Figure 4B-D**). The highest signal in the Hoechst 33342 assay at this concentration was detected in the case of the chromone-bearing fragment **27**. When analyzed in a concentration-dependent manner in the Hoechst 33342 assay, **27** proved to be as potent as inhibitor **1** (**Figure 4A** and **Table 1**). This is astonishing in so far, as it is a variant of only a part of compound **1**; it has a much lower MWT than **1**, hence a much higher ligand efficiency [46]. Therefore, we prepared a series of ABCG2 inhibitors derived from **27** (chromone series, compounds **39**-**43** and **48**-**50**). Fragments **12**, **16**, **18**, **19**, **20**, **22** and **25** inhibited ABCG2 to the same extent as fragment **4** (at 10 µM), namely by more than 50%. These fragments, as well as **13**, **14** and **21**, were selected as a basis for our second series of ABCG2 inhibitors (compounds **59**-**68**). Fragments **13**, **14** and **21**, although they inhibited ABCG2 by less than 50% (at 10 µM), were considered interesting: the inhibitors derived from **13** and **14** were likely to show higher solubilities (increase in the fraction of sp^3-hybridized carbon, disrupting planarity) and **21** bears a nitro group, reportedly conferring activity at ABCG2, which we hoped would influence larger molecules more than the fragments. Fragment **28**, differing from **27** only in the position of the carboxamido substituent at the chromone moiety, turned out to be instable in aqueous solution (data not shown), which is most probably the reason for its inactivity. All fragments were selective towards ABCG2. They did not show inhibition of ABCB1 and ABCC1 at 10 µM.

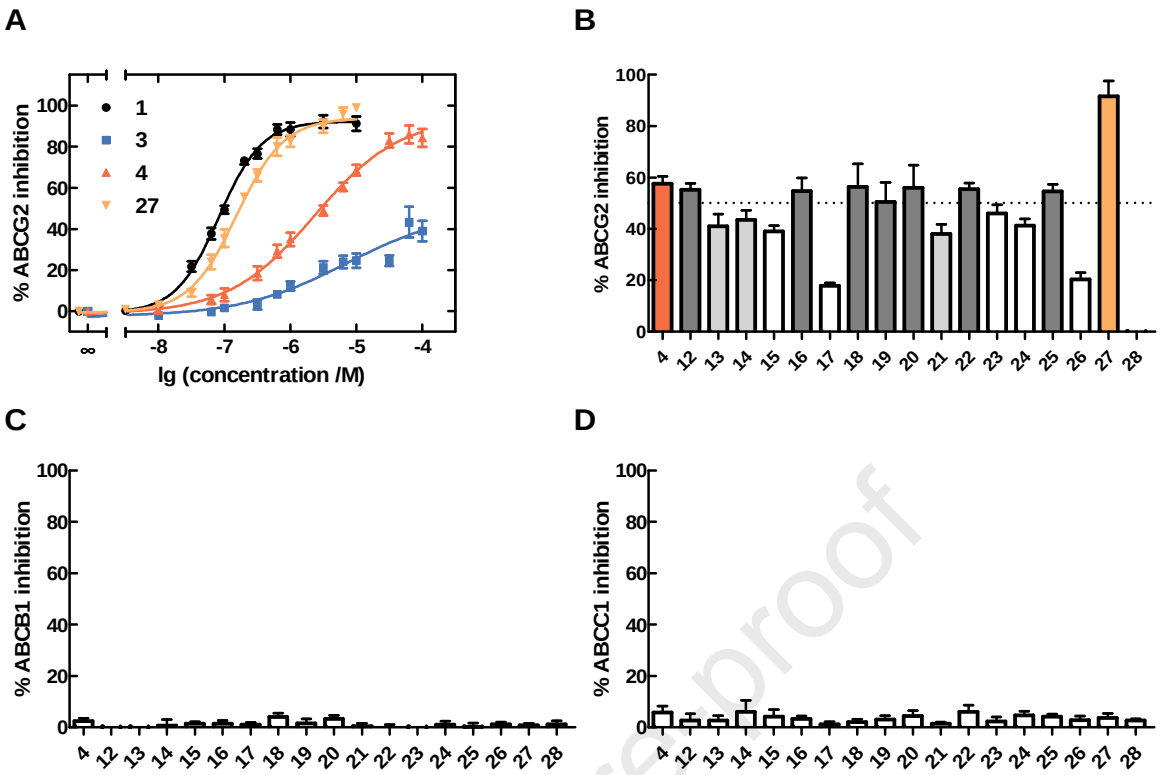

Figure 4. (A, B) Inhibition of ABCG2-mediated Hoechst 33342 efflux in MCF-7/Topo cells (A) by our previous tariquidar-related inhibitor **1**, the two substructures **3** and **4** and the novel fragment **27** (derived from **4**) in a concentration-dependent manner as well as (B) by compounds **4** and **12-28** at a concentration of 10 µM. The inhibition is expressed relative to the maximal effect in the presence of 10 µM FTC set to 100%. **(C, D)** Inhibition of ABCB1 (C) and ABCC1 (D) -mediated calcein-AM efflux in KB-V1 (C) and MDCK.2-MRP1 (D) cells by the fragments **4** and **12-28** at a concentration of 10 µM. The inhibition is expressed relative to the maximal effect in the presence of 10 µM tariquidar (C) and 30 µM reversan (D) set to 100%. Presented are mean values ± SEM from at least three independent experiments, each performed in triplicate.

The results of the transport assays for two series of inhibitors are depicted in **Figure 5** and **Figure 6**, showing exemplary concentration-response curves, and are summarized in **Table 1**. The introduction of polar groups into the structure of **27** via 'click' chemistry and the substitution of the methoxycarbonyl moiety by a propionyl group yielded the first subset (compounds **39**-**43**) of a chromone series. Compound **39**, which contains a 6,7-dimethoxy-1,2,3,4-tetrahydroisoquinoline moiety connected to the triazole ring with a phenylethyl linker (analogous to **1** and **2**), was only 65% effective. The comparison with fragment **27** (91% effective), as well as solubility considerations, suggested the introduction of much smaller moieties. Therefore, we conceived structures with only an ethylene or methylene linker between a polar group and the triazole ring. Compound UR-Ant116 (**40**), containing a morpholine ring, proved to be very effective (95%) and potent, showing an IC_{50} value of 312 nM (**Figure 5**). Compound UR-Ant121 **(41)**, bearing a pyrrolidine ring, was even a bit more potent (IC_{50} value of 158 nM), but less effective (70%) (**Figure 5**). The introduction of a hydroxyl group (compound **42**) decreased potency to an IC_{50} value above 1 µM. When a carboxylic acid (compound **43**) was introduced, the ability to inhibit ABCG2 was abolished. It

is very probable that the acid moiety, which on the one hand should increase solubility, on the other hand prevents the compound from entering the cell membrane.

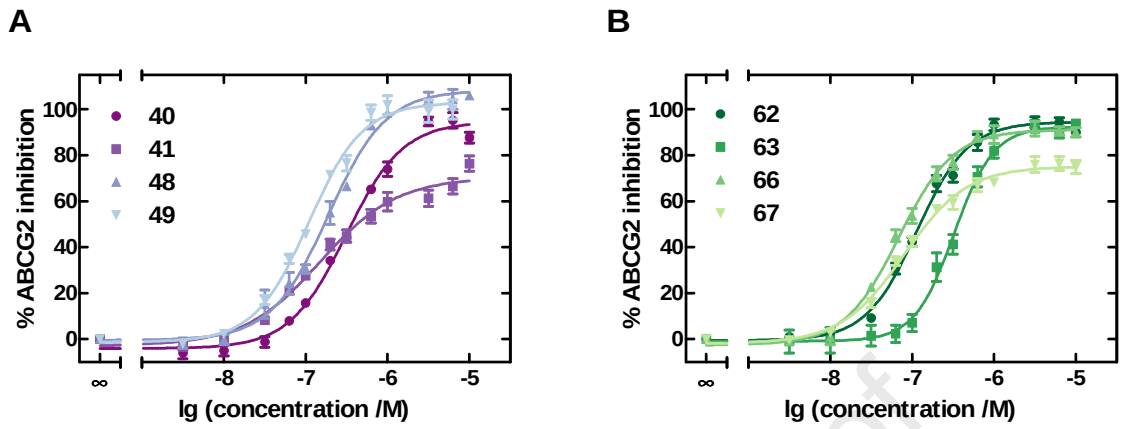

Figure 5. Concentration-dependent inhibition of ABCG2-mediated Hoechst 33342 efflux in MCF-7/Topo cells by (A) the chromones **40**, **41**, **48** and **49** as well as (B) the compounds **62**, **63**, **66** and **67**. The inhibition is expressed relative to the maximal effect in the presence of 10 µM FTC set to 100%. Presented are mean values ± SEM from at least three independent experiments, each performed in triplicate.

With respect to selectivity, the first subset of the chromone series showed interesting results. Compound **39** was selective for ABCG2. The smaller compounds **40**-**43**, though structurally extremely similar, behaved very differently. Whereas **41**, bearing a pyrrolidine ring, was selective for ABCG2, compound **40**, differing from **41** in the morpholine ring, was a triple ABCG2, ABCB1 and ABCG2 inhibitor (**Figure 6**). These two compounds could have different applications. For pharmacological tools selectivity is usually a necessity. For some clinical uses, however, inhibition of the three transporter subtypes may be advantageous. Especially ABCG2 and ABCB1 often have a concerted effect. Their expression overlaps at many physiological barriers (e.g. the GBB and the BBB), they share a number of clinically relevant substrates (such as topotecan), and a loss of function of one of these transporter subtypes can be compensated by an increase in the function of the respective other subtype [47,48]. Therefore a dual ABCB1/ABCG2 inhibitor may be necessary to overcome physiological barriers and MDR. Compound **42** showed low inhibition of ABCB1 and ABCC1. **43** was not only inactive at ABCG2, but also at ABCB1 and ABCC1. This is in agreement with the assumption that the acid is not capable of penetrating the cell membrane.

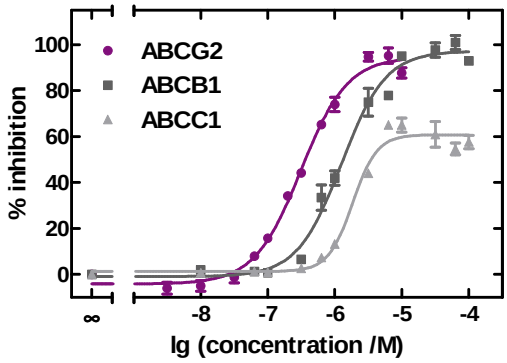

Figure 6. Concentration-dependent inhibition of ABCG2-mediated Hoechst 33342 efflux in MCF-7/Topo cells and of ABCB1 and ABCC1 -mediated calcein-AM efflux in KB-V1 and MDCK.2-MRP1 cells, respectively, by compound **40**. The inhibition is expressed relative to the maximal effect in the presence of 10 µM FTC, 10 µM tariquidar and 30 µM reversan, respectively, all set to 100%. Presented are mean values ± SEM from at least three independent experiments, each performed in triplicate.

The second subset (compounds **48**-**50**) of the chromone series features different substitution at the central phenyl ring and results from molecular docking studies with fragment **27**. Compounds UR-Ant131 (**48**), containing a morpholine ring, and UR-Ant132 (**49**) with a poyrrolidine ring were highly effective (over 100%) and highly potent in the Hoechst 33342 assay (IC_{50} values of 188 nM for **48** and 109 nM for **49**) (**Figure 5**); as was compound **50** (bearing a hydroxyl group), though a bit less so than the other two inhibitors (I_{max} 91%, IC_{50} 447 nM). Also these three compounds showed different selectivities. Contrary to **49** and **50**, which were specific ABCG2 inhibitors, compound **48** also inhibited ABCB1 and ABCC1, though only to a small extent (13% and 22%, respectively). It seems as if a morpholine ring can confer inhibitory potency at ABCB1 and ABCC1, since we observed the same effect – much more pronounced – in case of compound **40**.

Table 1. Inhibitory effects of our previous, tariquidar-related inhibitors **1** and **2**, the two substructures **3** and **4** and the novel fragment **27** (derived from **4**), as well as of the novel inhibitors **39**-**43**, **48**-**50** and **59**-**68** on the transport activity of ABCG2, ABCB1 and ABCC1.

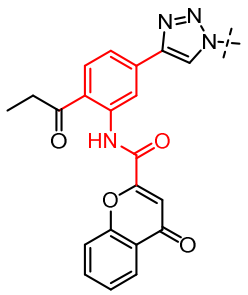

39-43

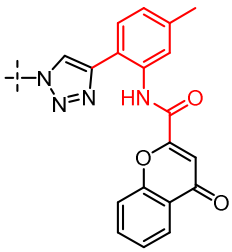

48-50

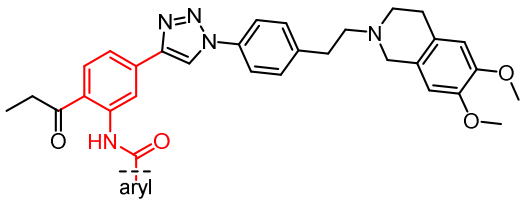

59-68

	ABCG2[a]		ABCB1[b]		ABCC1[c]	
Compound	IC_{50} [nM][d]	I_{max} [%][d,e]	IC_{50} [nM][d]	I_{max} [%][d,f]	IC_{50} [nM][d]	I_{max} [%][d,g]
1 (UR-MB108)[h]	79 ± 5	91 ± 2	inactive[i]	–	inactive	–
2 (UR-MB19)[h]	617 ± 179	90 ± 3	inactive	–	inactive	–
3 (UR-Ant74)	3606 ± 271	41 ± 5	inactive	–	inactive	–
4 (UR-Ant31)	1918 ± 482	86 ± 5	inactive	–	inactive	–
27 (UR-Ant56)	140 ± 14	91 ± 3	inactive	–	inactive	–
39 (UR-Ant71)	80 ± 25	65 ± 4	inactive	–	inactive	–
40 (UR-Ant116)	312 ± 14	95 ± 2	1342 ± 176	92 ± 3	2076 ± 163	66 ± 2
41 (UR-Ant121)	158 ± 22	70 ± 4	inactive	–	inactive	–
42 (UR-Ant127)	≥ 1102[j]	≥ 71[j]	≥ 2285[j]	≥ 41[j]	≥ 1963[j]	≥ 33[j]
43 (UR-Ant122)	inactive	–	inactive	–	inactive	–
48 (UR-Ant131)	188 ± 21	108 ± 3	≥ 1601[j]	≥ 13[j]	≥ 1469[j]	≥ 22[j]
49 (UR-Ant132)	109 ± 6	103 ± 4	inactive	–	inactive	–
50 (UR-Ant133)	447 ± 27	91 ± 4	inactive	–	inactive	–
59 (UR-Ant124)	249 ± 20	70 ± 2	inactive	–	inactive	–
60 (UR-Ant115)	180 ± 15	63 ± 3	inactive	–	inactive	–
61 (UR-Ant110)	166 ± 24	81 ± 6	≥ 9972[k]	≥ 19[k]	inactive	–
62 (UR-Ant68)	116 ± 9	95 ± 2	inactive	–	inactive	–
63 (UR-Ant105)	322 ± 32	92 ± 2	inactive	–	inactive	–
64 (UR-Ant108)	116 ± 21	68 ± 5	≥ 2775[k]	≥ 13[k]	inactive	–
65 (UR-Ant112)	328 ± 48	75 ± 1	≥ 18450[k]	≥ 14[k]	inactive	–
66 (UR-Ant111)	70 ± 7	91 ± 2	inactive	–	inactive	–
67 (UR-Ant113)	82 ± 10	75 ± 3	inactive	–	inactive	–
68 (UR-Ant62)	120 ± 8	78 ± 1	inactive	–	inactive	–

[a] Hoechst 33342 microplate assay, using ABCG2-expressing MCF-7/Topo cells.
[b] Calcein-AM microplate assay, using ABCB1-expressing KB-V1 cells.
[c] Calcein-AM microplate assay, using ABCC1-expressing MDCK.2-MRP1 cells.
[d] Mean values ± SEM from at least three independent experiments, each performed in triplicate.
[e] Maximal inhibitory effect (I_{max}) relative to the response to FTC at a concentration of 10 µM (100%).
[f] Maximal inhibitory effect (I_{max}) relative to the response to tariquidar at a concentration of 10 µM (100%).
[g] Maximal inhibitory effect (I_{max}) relative to the response to reversan at a concentration of 30 µM (100%).
[h] Data taken from our previous study [28].
[i] Inactive: response ≤ 10% up to a concentration of 100 µM.
[j] No plateau was reached at the kinetic solubility limit (3 µM); minimum IC_{50} values and I_{max} values were stated.
[k] No plateau was reached up to a concentration of 100 µM; minimum IC_{50} values and I_{max} values were stated.

The second series (compounds **59**-**68**) originating from the fragment screening, are analogs of compound **1**, the quinoline group being substituted with aryl moieties that compared favorably in the fragment analysis. They all showed IC_{50} values in the two- to low three-digit nM range. The most effective substances from this series, with an I_{max} value of over 90%, were compound **62**, with a 2-chloropyridine moiety, compound **3**, containing a 2-methoxypyridine group, and compound **66**, featuring 2-nitropyridine, which was the most potent substance of this series with an I_{50} value of 70 nM (**Figure 5**). Compound **61**, comprising a 2-methylpyridine moiety, was with 81% only a little less effective. Compounds **59**, **60**, **64**, **65**, **67** and **68** showed efficacies somewhat below 80%. Compound **67**, with a 2-aminopyridine group, was the most potent among the latter substances, showing an IC_{50} value of 82 nM (and an I_{max} value of 75%) (**Figure 5**). All members of this series were highly selective for ABCG2, except for compounds **61**, **64** and **65**. The latter also inhibited ABCB1, but only by less than 20% and only at very high concentrations (100 µM). They showed a clear preference for ABCG2 and thus are rather selective.

2.3.2 Cytotoxicity and Reversal of Drug Resistance

The cytotoxicity and the ability to reverse the resistance of MCF-7/Topo cells toward the cytostatic drug topotecan was investigated exemplarily in a kinetic chemosensitivity assay for the inhibitors **40** and **48** as representatives of the two subsets of the chromone series and compound **63**, a member of the second series. As shown in **Figure 7**, against MCF-7/Topo cells, compound **40** was nontoxic up to a concentration of 1 µM and exhibited a cytotoxic effect only at higher concentrations. Upon incubation with topotecan at a concentration of 100 nM, the cells were not affected due to their resistance, whereas the addition of **40** at per se nontoxic concentrations entirely reversed the resistance. Inhibitor **48** did not show any cytotoxicity, even at a concentration as high as 10 µM. Analogous to **40**, **48** was able to reverse topotecan resistance; the same was true of inhibitor **63**, when administered at a nontoxic concentration, which was up to 1 µM. At higher concentrations **63** displays a cytotoxic effect. In sum, this assay disclosed that the compounds analyzed prevented the topotecan efflux, which is in accordance with the results of the Hoechst 33342 transport assay.

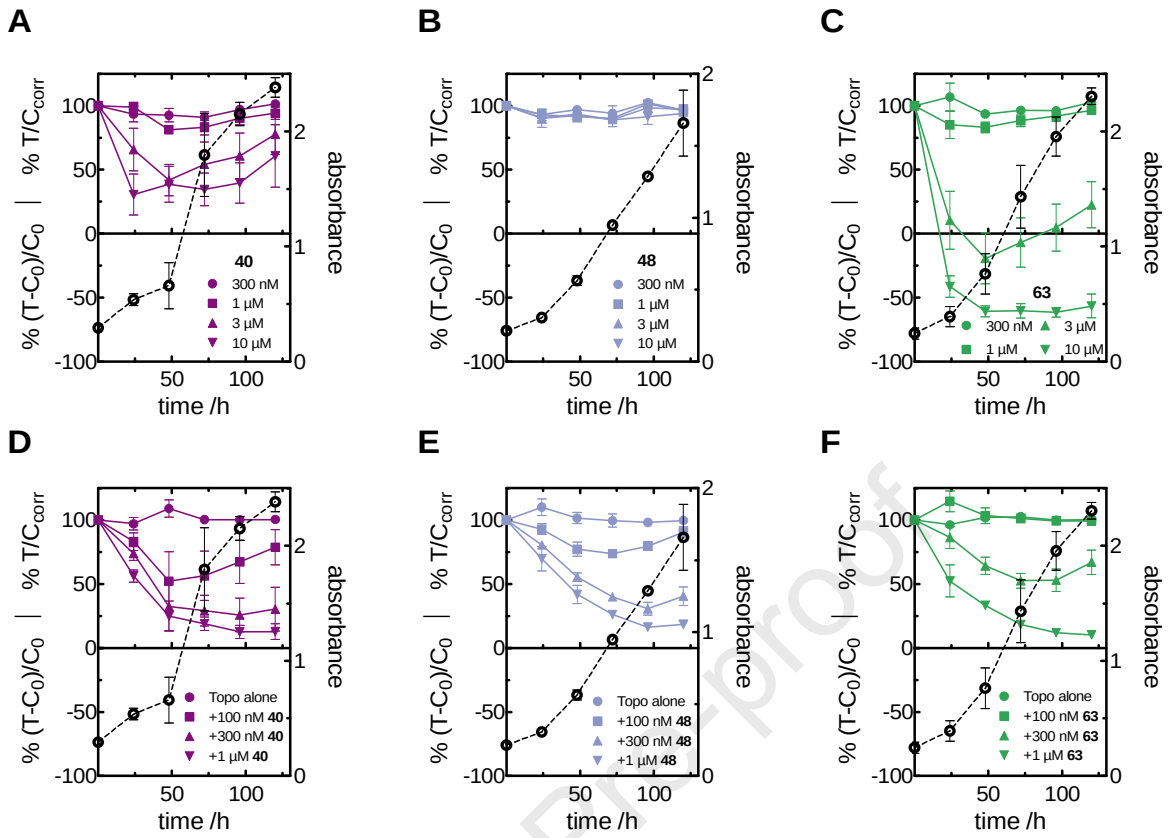

Figure 7. (A-C) Antiproliferative activities of the inhibitors **40** (A), **48** (B) and **63** (C) against MCF-7/Topo cells upon long-term incubation. **(D-F)** Reversal of ABCG2-mediated drug resistance against topotecan on proliferating MCF-7/Topo cells: effect of 100 nM topotecan (Topo) alone and in combination with different concentrations of **40** (D), **48** (E) or **63** (F). Antiproliferative effects correspond to the left y-axes. The growth curves of untreated control cells (open circles) correspond to the right y-axes. Data are mean values ± SEM of two to three independent experiments, each performed in octuplicate.

2.3.3 Effect on the ATPase Activity

For comprehensive biological characterization, we investigated our most advantageous transport inhibitors in terms of potency and solubility, UR-Ant116 (**40**), UR-Ant121 (**41**), UR-Ant131 (**48**) and UR-Ant132 (**49**), in an ATPase assay, which gives information on the type of inhibition. We performed the assay with membrane preparations of human ABCG2 overexpressing MCF-7/Topo breast cancer cells in order to provide a membrane environment for native protein structure and function. Transport of substrates by ABCG2 is an alternating process, whereby the substrate-bound, inward-open conformation is converted to an outward-facing state that can release the substrate to the outside [30]. ABCG2 gains the energy for this process by ATP-hydrolysis to ADP and inorganic phosphate. The latter was determined by a molybdenum blue reaction after incubation of the membranes for a certain period of time (with and without a transport inhibitor) as an estimate for the ABCG2-associated ATPase activity, thereby assessing the influence of test compounds on the ATPase activity of ABCG2. In the absence of an ATPase stimulating agent, ABCG2 typically displays basal ATPase activity, presumably induced by endogenous substrates (e.g. lipids) [49] present in the

membrane preparations, which was set to zero in our assay. As depicted in **Figure 8A**, both compounds **40** and **41**, belonging to the first subset of the chromone series, at concentrations of 1 µM and 10 µM, suppressed the ATPase activity to a level even below the basal ATPase activity. This led to the conclusion that these two compounds are not substrates of ABCG2. It has been shown that the inhibition of the ATPase and of the transport activity are closely connected. A recent cryo-EM study [29] suggested that ABCG2 transport inhibitors, including one member of our preceding tariquidar analogs (UR-MB136), bind to a central multidrug binding site located in the transmembrane domain, lock the inward-facing conformation of ABCG2 and inhibit the ATPase activity through conformational coupling with the cytoplasmic nucleotide-binding domain. Based on these results, it can be assumed that the inhibition of the ATPase activity by compounds **40** and **41** contributes to the overall inhibition of ABCG2 transport. In contrast to the compounds **40** and **41**, the transport inhibitors **48** and **49**, members of the second subset of the chromone series displaying different substitution at the central phenyl ring, showed a very distinct behavior in the ATPase assay – they did not suppress, but stimulate the ATPase activity of ABCG2 (at concentrations of 1 µM and 10 µM) and therefore are most likely substrates of the transporter rather than ATPase inhibitors. In order to find out to which degree they activate the ABCG2 ATPase activity, we determined concentration-response curves of the two compounds. As shown in **Figure 8B**, **48** and **49** exhibited I_{max} values of 46% and 29%, respectively, and potencies of 96 nM and 62 nM, respectively. It is conceivable that they compete with other substrates, such as Hoechst 33342, for transport and thereby reduce their transport. However, they do not fully activate the ATPase activity; it can also be supposed that by being transported more slowly, they occupy the multidrug binding site of the transporter, so that it is not at disposal for other substrates.

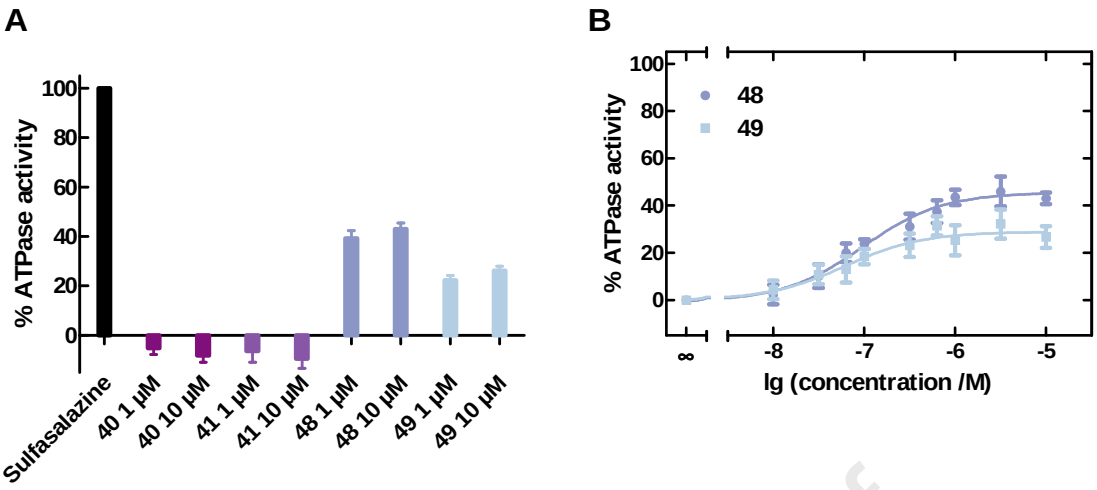

Figure 8. Stimulation or suppression of the ATPase activity in ABCG2-expressing MCF-7/Topo membrane preparations by the compounds **40**, **41**, **48** and **49** at a concentration of 1 µM and 10 µM (A) and concentration-dependent stimulation of the ATPase activity by the compounds **48** and **49** (B). The effect is expressed relative to the basal ATPase activity (0%) and the maximal stimulatory effect in the presence of 30 µM sulfasalazine set to 100%. Presented are mean values ± SEM from at least three independent experiments each performed in triplicate.

It is interesting that minor structural changes have such an impact on the type of inhibition. This shows that it is possible to modulate the inhibition type according to the needs of the desired application. ATPase activators and suppressors may have different applications. Whereas ATPase activators deplete the cell of ATP, a compelling effect when addressing resistant tumor cells [50], ATPase suppressors do not interfere with the ATP balance of the cell.

2.3.4 Stability in Blood Plasma

Having analyzed the biological activity and selectivity of our inhibitors, investigations on their drug-like properties were pending. After studying cytotoxicity we determined the stability in blood plasma, which is a precondition for in vivo studies. Chromone is a structural element quite common in natural products and drugs and can be considered a privileged scaffold [51,52] in drug discovery, not least due to its synthetic availability, structural diversity and low toxicity (confirmed in our cytotoxicity assay, using MCF-7/Topo cells, see **Figure 7**). However, chromones may be susceptible to hydrolysis, depending on the substitution pattern. 3-Substituted chromones are very reactive towards the attack of nucleophiles, such as water [53]. We observed this behavior with fragment **28**, a 3-substituted chromone, which hydrolyzed rapidly in aqueous solution, explaining the lack of biological activity. By contrast, fragment **27**, a chromone substituted in 2-position, exhibited excellent inhibition of ABCG2 and was the foundation of our chromone series. Exemplarily of this series, compound **49** was incubated in human plasma and analyzed via HPLC with UV detection at 220 nm (**Figure 9A**). The peak area of **49** decreased by about 58% over a period

of 24 hours, yet no additional peaks were detected. On the off chance that a possible degradation product may not be detectable by this method (due to lacking UV-absorption or retention), the samples were also analyzed by HPLC-MS coupling (0 h and 24 h). Also with this hyphenated technique, applying a different gradient, no additional peaks were detected (data not shown). Therefore, we attributed the decrease in the peak area to adsorption, either to the vial surface or to plasma proteins, and concluded that **49** is in fact stable in blood plasma. Moreover, the main decrease in peak height occurred in the first five hours and after that, the peak area remained almost unchanged, which supports our assumption that the decrease is due to adsorption, not to hydrolysis.

Furthermore, as a representative of the second series, inhibitor **65** was studied in the same manner (**Figure 9B**). The situation was the same as with compound **49** – the peak area of **65** decreased but no additional peaks were detected, also upon HRMS analysis (data not shown). Hence, we again concluded that the compound was adsorbed to a certain extent.

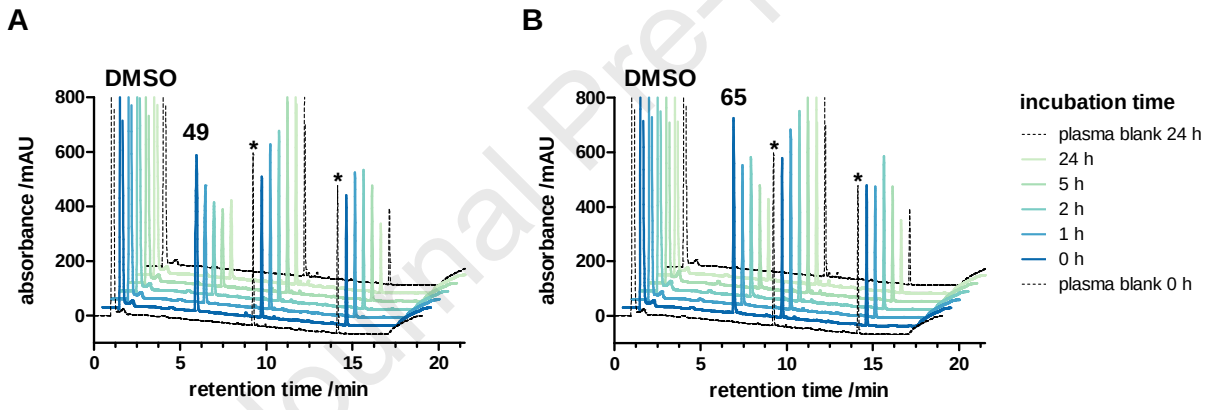

Figure 9. Chromatograms illustrating the stability of the compounds **49** (A) and **65** (B) upon incubation in human blood plasma at 37 °C over a period of 24 h. RP-HPLC analysis, UV detection at 220 nm. *Blood plasma constituents.

2.4 Aqueous Solubility

When determining the solubility of chemical entities, it is fundamental to understand the distinction between thermodynamic and kinetic solubility. Thermodynamic – or equilibrium – solubility is defined as the maximum concentration of a solute in a solvent in a state of complete thermodynamic equilibrium, i.e. a saturated solution at equilibrium with an excess of undissolved solid and at a fixed temperature and pressure [54,55]. It is usually determined by the classical shake-flask method (using a solid in a buffer) with subsequent HPLC-analysis [1,8,13,56]. By contrast, in kinetic solubility assays no equilibrium is reached. Most often the compound, 'pre-dissolved' in DMSO, is added into an aqueous buffer and precipitation is measured turbidimetrically or nephelometrically after a short period of time [57-59]. The concentration of the compound in the buffer at which a precipitate appears is termed kinetic

solubility [1,8,13]. Unlike thermodynamic solubility assays, kinetic assays can be performed in microplates in high throughput and they are useful to verify concentration-response data – making sure that precipitation does not occur on the time scale of the biological assay. They are also used as an early estimate of solubility in drug discovery [1,8,58]. However, the apparent solubility in a kinetic assay is always – sometimes dramatically – higher than the thermodynamic 'true' solubility and therefore should not be used for decision-making, otherwise the optimization process may be driven towards the synthesis of compounds with the slowest precipitation rather than the highest solubility [1,2,8,60].

Here, we established both a kinetic solubility assay mainly to verify our biological data and a thermodynamic solubility assay in order to rank our ABCG2 inhibitors in terms of solubility and thereby to assess if our efforts met our objective – potent ABCG2 inhibitors with improved solubility.

2.4.1 Kinetic Solubility

Assay Adaptation. We conducted the kinetic solubility assay in microplates under conditions identical to those in the biological assays. Inhibitor solutions in DMSO at increasing concentrations were diluted 1:100 in the respective aqueous buffer, resulting in a uniform DMSO concentration (1%) in each well. The plates were incubated at 37 °C for two hours – the time span of the Hoechst 33342 assay, which is the most time-consuming assay among the ATPase and transport assays. While handling the plates, attention was paid to avoiding scratches on the plates that might have interfered with the readouts. Then the extinction was measured as a function of the inhibitor concentration. The extinction of electromagnetic radiation, when passed through a suspension, is due to the processes of absorption, scattering, diffraction and reflection. When the extinction is measured at a wavelength at which the test compound does not absorb any light, a sharp increase in the extinction values at a certain concentration arises from scattering due to precipitation, corresponding to the solubility limit of the respective compound [57]. At that point, the clear solution turns into a turbid suspension containing solid particles.

Since ABCG2 inhibitors show poor solubility, we strove for a detection limit as low as possible, thus a signal intensity as high as possible. Therefore, we needed to adjust the changeable assay parameters, namely sample volume and measurement wavelength, accordingly. In order to get an estimate for the detection limit we required a substance with extremely low aqueous solubility as a reference. We chose coronene, a polycyclic aromatic compound comprising six peri-fused benzene rings, which shows an aqueous solubility as low as 0.5 nM [61] (detected fluorometrically). When performing the assay with this compound, it

can be assumed that the concentration at which the sharp increase in extinction occurs indicates the detection limit of the assay rather than the solubility limit of coronene, because coronene is practically insoluble in water and experiments showed that precipitation takes place quickly – after the addition of the DMSO stock solution to the buffer the concentration-extinction curve was measured repeatedly and remained almost constant for 24 hours (data not shown). Using coronene, we explored the effects of the sample volume and of the wavelength on the signal intensity, thus the detection limit of the assay. As expected, the signal intensity increased with the sample volume (data not shown). Therefore, we employed the highest volume possible per microplate well in the assay, namely 300 µL. For analyzing the dependence of the signal intensity on the wavelength, we considered the spectral properties of coronene, DMSO and polystyrene (microplate material). The latter shows absorption between 200 nm and 290 nm, which decreases rapidly above 290 nm [62]. DMSO exhibits a sharp absorption maximum at a wavelength of around 250 nm and practically no absorption above 265 nm [63]. The main absorption bands of coronene are located between 300 nm and 350 nm and there is only very low absorption above 350 nm [64]. Therefore, we performed the experiment at different wavelengths ranging from 380 nm to 830 nm, where the aforementioned compounds do not absorb radiation (**Figure 10A**). Light scattering drastically decreases with increasing wavelength, though this effect depends on the particle size and is more pronounced for small particles [65]. Accordingly, when measuring the extinction as a function of the coronene concentration, we found the highest signal intensity at a wavelength of 380 nm and the lowest at 830 nm. To find the lowest wavelength compatible, we measured the UV/VIS absorption spectra of our inhibitors (examples thereof depicted in **Figure 10B**) and found that they have a cut-off wavelength of 380 nm, which we chose as measurement wavelength for our assay.

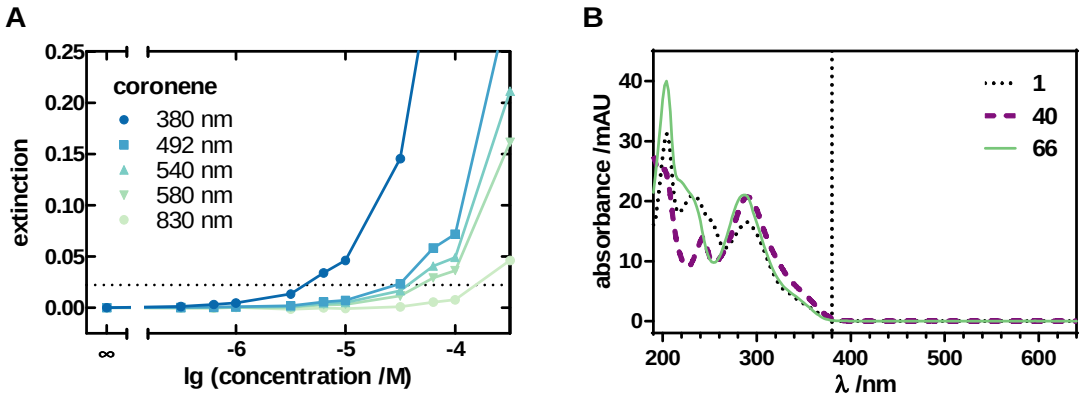

Figure 10. (A) Effect of the wavelength on the signal intensity in a kinetic solubility assay: extinction (mainly due to scattering) as a function of the concentration of the 'insoluble' standard coronene at different wavelengths. The data were normalized to the blank value. Presented are mean values ± SEM from one experiment performed in octuplicate. **(B)** UV/VIS absorption spectra of the inhibitors **1**, **40** and **66**, revealing a shared cut-off wavelength of 380 nm.

By analogy with a recently published study [66] covering the solubility of a detergent (sodium lauroyl isethionate), we estimated the kinetic solubility of the test compounds as the highest concentration at which more than 95% of the radiation is transmitted, i.e. the extinction is lower than 0.0223, the data having been normalized to the blank value (1% DMSO in buffer). The threshold is indicated as a dashed line in **Figure 10A** and **Figure 11**. In the case of coronene, the highest concentration below the threshold was 1 µM, which we identified as the detection limit. It should be noted that the detection limit determined in this assay is only applicable under the assumption that the inhibitors precipitate with particle size and form similar to coronene.

Assay Results. We examined our previous inhibitor UR-MB108 (**1**), fragment **27**, and all our novel inhibitors (**39**-**43**, **48**-**50** and **59**-**68**) in the kinetic solubility assay, using PBS (pH 7.4) as a solvent. We included coronene in every batch of assays as a control for precipitation. Exemplary concentration-extinction curves are depicted in **Figure 11**. The estimated kinetic solubility limits are listed in **Table 2**.

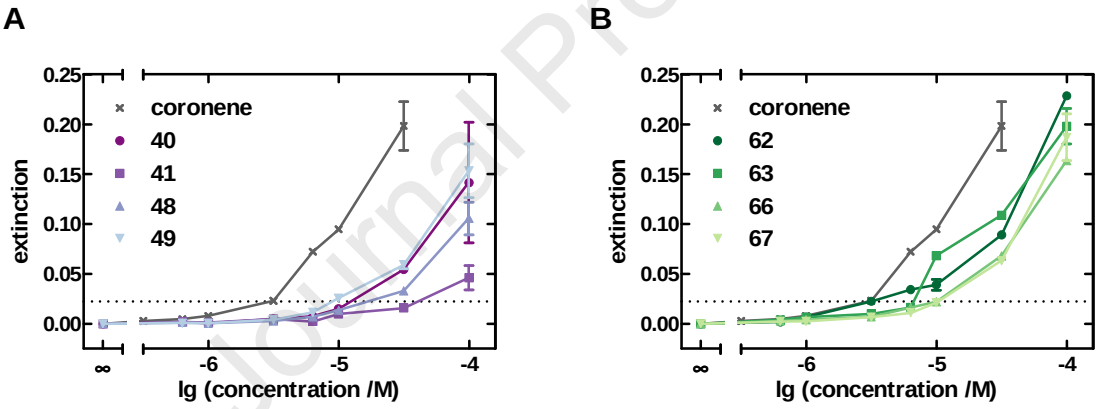

Figure 11. Concentration-dependent extinction (at 380 nm) due to scattering in a kinetic solubility assay in PBS caused by (A) the chromone inhibitors **40**, **41**, **48** and **49** as well as (B) the inhibitors **62**, **63**, **66** and **67**. The data were normalized to the blank value. Presented are mean values ± SEM from two to three independent experiments, each performed in triplicate.

We compared the concentration-dependent curves in the functional assays with the kinetic solubility limits in order to decide if the biological data were compromised by precipitation (c.f. **Figure S1** in the Supporting Information). If a curve reached a plateau before the solubility limit was achieved, we concluded that the curve was unaffected by solubility constraints and that the values derived from the curve (I_{max} and IC_{50}) are valid. Our previous inhibitor **1** and fragment **27** showed a solubility limit of 3 µM and 10 µM, respectively. The curves of both compounds reached a plateau in the Hoechst 33342 transport assay at around 1 µM, meaning that the biological data are reliable. The chromone inhibitors exhibited solubility limits between 3 µM and 30 µM and all of them, except for one, achieved a plateau in the Hoechst 33342 assay before the solubility limit was reached. Only the curve of

compound **42**, which was less potent than the other chromones, did not reach a plateau; the values increased up to a concentration of 3 µM and then suddenly dropped. This reflects the results of the kinetic solubility assay, according to which the solubility limit was reached at 3 µM. This consistency indicates that the kinetic solubility assay is reliable. We marked insufficient solubility as the cause for the incomplete curve in a footnote to **Table 1**. We also investigated some of our chromone inhibitors – compounds **40**, **41**, **48** and **49** – in the ATPase assay. Since the highest concentration employed there was 10 µM, the ATPase data are largely not compromised by insufficient solubility.

Our second series of inhibitors, compounds **59**-**68**, showed kinetic solubilities up to 10 µM. The curves of compounds **60**, **63** and **65**-**68** all reached a plateau in the Hoechst 33342 assay at concentrations lower than the respective kinetic solubility limit. The curves of compounds **59**, **61** and **64** also reached a plateau, although this was at concentrations that slightly exceeded their respective kinetic solubility limit. It is possible that with higher solubility, their I_{max} values might be slightly higher. The curve of compound **62** reached a plateau at about 3 µM and this inhibitor exhibited a solubility limit of 1 µM, which is around the detection limit. The first values of the concentration-extinction curve coincided with the ones from the control coronene but a strong increase occurred only at higher concentrations, at around 10 µM. Therefore it is improbable that the biological data of compound **62** are impaired.

We did not only test our substances for interaction with ABCG2, but we also assessed their selectivity and therefore examined them for inhibition of ABCB1 and ABCC1 in the calcein-AM assay. Most of the inhibitors analyzed were selective towards ABCG2 or just exhibited very low inhibitory potency at the other two transporters. At concentrations higher than their solubility limits – we studied the inhibitors at concentrations up to 100 µM – they might appear more selective than they actually are. Since this concerns only quite high concentrations, however, we considered this not very relevant. Three compounds were not selective, namely the chromones **40**, **42** and **48**. Regarding compound **42**, the situation is the same as with the Hoechst 33342 assay; no plateau was reached at the solubility limit (as we indicated in the footnote to **Table 1**). The curves of compound **40**, which is a triple ABCB1/ABCC1/ABCG2 inhibitor, plateaued in both calcein-AM assays before the solubility limit of 10 µM was reached. Compound **48** also showed some potency at ABCB1 and ABCC1, but did not reach a plateau in the calcein-AM assays at concentrations below the solubility limit of 10 µM, which we indicated in **Table 1**.

Altogether, with a few exceptions, the biological data were not affected much by kinetic solubility limits.

Table 2: Estimated kinetic solubility limits of our previous tariquidar analog **1**, fragment **27**, and the chromone inhibitors (**39**-**43**, **48**-**50**) as well as the second series of inhibitors (**59**-**68**).

Compound	Kinetic Solubility [µM][a]	Compound	Kinetic Solubility [µM][a]
1 (UR-MB108)[h]	3	**59** (UR-Ant124)	3
27 (UR-Ant56)	10	**60** (UR-Ant115)	7
39 (UR-Ant71)	7	**61** (UR-Ant110)	3
40 (UR-Ant116)	10	**62** (UR-Ant68)	1
41 (UR-Ant121)	30	**63** (UR-Ant105)	7
42 (UR-Ant127)	3	**64** (UR-Ant108)	3
43 (UR-Ant122)	10	**65** (UR-Ant112)	7
48 (UR-Ant131)	10	**66** (UR-Ant111)	10
49 (UR-Ant132)	7	**67** (UR-Ant113)	10
50 (UR-Ant133)	3	**68** (UR-Ant62)	7

[a] Highest concentration in the kinetic solubility assay in PBS (data normalized to the blank value), at which transmission was higher than 95%, i.e. the extinction was lower than 0.0223.

The buffer used in the transport assays also contained serum albumin. Since this can influence precipitation, we also performed kinetic solubility assays in a buffer containing bovine serum albumin (BSA). We found that the addition of BSA did not change the data significantly, which is shown exemplarily for compound **1** in **Figure S2** in the Supporting Information.

2.4.2 Thermodynamic Solubility

Assay Adaption. To determine thermodynamic solubility the traditional shake-flask technique was modified. In the course of the optimization of the assay, we repeatedly faced major challenges due to the high lipophilicity and low solubility range of ABCG2 inhibitors.

We scaled the procedure down in order to facilitate handling and to minimize the amount of substance required. On downscaling it should be borne in mind that the surface to volume ratio is larger the smaller the flask. Therefore adsorption of the solute to the vial surface may have a greater effect on the thermodynamic equilibrium between the saturated solution and the undissolved solid. To minimize adsorption we tested different vial materials regarding the ability to adsorb compounds such as **1**. Indeed there were distinct differences. We found the most pronounced adsorption with untreated glass vials (maybe due to ionic interactions between the negatively charged silanol glass surface and the positively charged, protonated heterocycle in **1**), followed by untreated polypropylene (PP), ‘siliconized’ PP (i.e. PP treated with a siliconizing agent) and the least with ‘siliconized’ glass, which we chose for the assay (graph see **Figure S3** in the Supporting Information).

With respect to in vitro as well as in vivo studies we used PBS at a pH value of 7.4 as a solvent. This is the usual pH value in the biological assays and the pH value in the small intestine as well as many other body fluids, such as blood plasma, lymph, cerebrospinal fluid and cytoplasm. It is common practice to use an aqueous buffer as a simplistic surrogate of the intestinal content in solubility studies [2,67]. Typically, the sample is prepared by adding solid to the buffer. This turned out to be practically impossible with our substances – they showed very poor wettability and tended to float on the surface, even after shaking, making it impossible to take out a homogeneous aliquot for HPLC analysis without some of the solid adhering to the pipette tip. This behavior may be attributed to their lipophilicity. Unfortunately, the lipophilicity also made it impossible to remove floating substance by filtration – adsorption to the filter (different materials tested) was so pronounced that not only the floating substance, but also the dissolved compound was removed from the solution and after filtration there was no signal detectable by HPLC. We solved this problem by adding a stock solution in DMSO to the buffer instead of adding solid. Of course, the presence of DMSO influences the solubility of a compound. It has been shown that a DMSO content over 5‰ can distort the results of thermodynamic solubility assays [68]. So we kept the DMSO content at only 1‰.

After the sample preparation, we incubated it in a shaker at 25 °C. Studies showed that a thermodynamic equilibrium is usually established after 24 hours of stirring [69]. We shook our samples for 36-40 hours to make sure an equilibrium had been reached and then allowed sedimentation for another 24 hours. In case a compound did not sediment properly, we centrifuged the sample.

Another challenge associated with the low solubility and high lipophilicity of the inhibitors was the transfer of the samples into the HPLC vials. After transferring compound **1**, we did not detect any peak and found out that the reason was adsorption of **1** to the pipette tip. After pipetting the sample into an HPLC vial containing acetonitrile and rinsing the tip, a peak was detectable.

Having established a procedure for the thermodynamic solubility assay, we validated it with haloperidol as a reference substance. The solubility of the latter is referred to as 37 µM in literature [70]. We determined a solubility of 40 ± 1 µM.

Assay Results. We investigated fragment **27**, our novel inhibitors (**39**-**42**, **48**-**50** and **59**-**68**) as well as our previous tariquidar analog **1** in the thermodynamic solubility assay (**Table 3**). As already stated in the introduction, compound **1** exhibited an equilibrium solubility of only 78 nM. Furthermore it violates two of the Ro5 due to its size and high clogP. The first series

of inhibitors is based on fragment **27**, a substructure of **1**, containing a chromone instead of a quinoline moiety. Though much smaller, **27** was equipotent with **1**. Its solubility, however, with 109 nM, was not much higher than the solubility of **1**, despite its low molecular weight and conformity with the Ro5. This can probably be attributed to the lack of a protonatable nitrogen. The inhibitors derived from fragment **27** all contain a polar or ionizable moiety. Compounds **39**-**43**, the first subset of the chromone inhibitors, display very different solubilities. Merging **27** with fragment **3** led to the inhibitor **39**, which was only slightly more soluble than **1** (149 nM). However, when far smaller polar moieties were introduced (compounds **40**-**43**), the solubility could be enhanced markedly and in contrast to **39** the compounds complied with the Ro5, or in case of **40**, almost complied (only the MWT was slightly higher than 500 g/mol). Compounds **41** and **42** both contain a heterocycle (morpholine in **40** and pyrrolidine in **41**) and exhibit solubilities of ca. 1 and 1.5 µM, respectively – 13-fold and 19-fold the solubility of inhibitor **1**. The introduction of a hydroxyl group into compound **42** increased the solubility to 575 nM. Compound **43**, containing a carboxyl group, was not measured because it did not inhibit ABCG2. The second subset of the chromone inhibitors, compounds **48**-**50**, differs structurally from the first subset, the main difference being the absence of an acyl moiety. The inhibitors obey the Ro5 and, here again, the compounds containing an ionizable ring – **48** and **49** – showed high solubilities (1.1 and 1.3 µM, respectively) compared to **1**. The introduction of a hydroxyl group (in compound **50**) did not increase the solubility.

The second series of inhibitors (**59**-**68**) is structurally more similar to compound **1**. The compounds are analogs of **1**, the quinoline moiety being replaced by other ring structures. They have MWTs similar to **1** and, therefore, violate at least one Ro5. However, we were able to increase the fraction of sp^3-hybridized carbon or decrease the clogP values compared to **1**, i.a. by introducing polar groups. The latter strategy, of course, also led to an increase in the number of H-donors or H-acceptors and in some cases to Ro5 violations.

Compound **59**, containing a naphthalene ring and designed with regard to improved rotation around the amide bond and reduced planarity, did not show improved solubility. Compound **60** contains a tetrahydroquinoline ring to reduce aromaticity, thus planarity and π-π stacking and ultimately crystal packing. This substitution did not increase the solubility, either. However, when the phenyl ring in the quinoline moiety was replaced by a smaller group containing sp^3-hybridized carbon, namely a methyl group (compound **61**), the solubility was six-fold increased to 445 nM. The introduction of polar moieties, replacing the phenyl ring, yielded different results. Compound **62**, an organic chloride, did not display increased

solubility. Though electronegative, chlorine confers lipophilicity due to its size. Also the introduction of a methoxy group, attached in different positions in compounds **63** and **64**, did not solve the solubility problem; neither did the attachment of a nitro (in **66**) or an amino (in **67**) group. Here, a general problem of increasing solubility by introducing polar groups becomes apparent – on one hand, polarity will indeed be increased by this approach and the heteroatoms can form stabilizing H-bonds with water, but on the other hand also polar intermolecular interactions may be increased. This could lead to enhanced crystal packing, counteracting the solubilizing effect of the polar groups. Fortunately, this strategy proved successful, nevertheless. Compound **65**, displaying a hydroxyl group, is over ten times more soluble than **1** (855 nM). We find it surprising that the introduction of an amino group did not have the same effect. Lastly, the replacement of the quinoline moiety by a slightly smaller and less lipophilic benzofuran ring (in **68**) did not improve the solubility.

Table 3. Ro5 compliance and thermodynamic solubilities of our previous tariquidar analog **1**, fragment **27**, and the chromone inhibitors (**39**-**43**, **48**-**50**) as well as the second series of inhibitors (**59**-**68**).

Compound	MWT [g/mol]	ClogP[a]	H-Donors	H-Acceptors	Ro5 Violations	Thermodynamic Solubility [nM][b]
1 (UR-MB108)	666.77	5.42	1	10	2	78 ± 5
27 (UR-Ant56)	402.20	3.23	1	6	0	109 ± 18
39 (UR-Ant71)	683.75	3.64	1	11	2	149 ± 36
40 (UR-Ant116)	501.53	1.75	1	10	(1)	999 ± 189
41 (UR-Ant121)	485.53	2.81	1	9	0	1483 ± 383
42 (UR-Ant127)	432.43	1.51	2	9	0	575 ± 144
43 (UR-Ant122)	446.41	1.85	2	10	0	n. d.[c]
48 (UR-Ant131)	459.50	1.71	1	9	0	1144 ± 203
49 (UR-Ant132)	443.50	2.76	1	8	0	1228 ± 106
50 (UR-Ant133)	390.39	1.47	2	8	0	< 100
59 (UR-Ant124)	665.78	5.63	1	9	2	< 100
60 (UR-Ant115)	670.80	5.41	1	10	2	< 100
61 (UR-Ant110)	630.74	4.46	1	10	1	445 ± 48
62 (UR-Ant68)	651.15	4.47	1	10	1	< 100
63 (UR-Ant105)	646.73	5.25	1	11	3	< 100
64 (UR-Ant108)	646.73	4.21	1	11	2	119 ± 29
65 (UR-Ant112)	632.71	4.30	2	11	2	855 ± 242
66 (UR-Ant111)	661.71	4.05	1	13	2	< 100
67 (UR-Ant113)	631.72	3.60	3	11	2	< 100
68 (UR-Ant62)	655.74	5.04	1	10	2	< 100

[a] Calculated LogP values, using ACD/Structure Designer.
[b] Thermodynamic solubility assay: shake-flask experiment in PBS with subsequent HPLC analysis. Mean values ± SEM from at least six independent experiments, each performed in duplicate.
[c] n. d.: not determined.

When comparing the two series of inhibitors it becomes obvious that the chromone inhibitors, which are smaller and structurally more different from **1**, are superior to the members of the

second series in terms of solubility and Ro5 compliance. The fragment-based approach led to the discovery of fragment **27**, which is a very potent and effective ABCG2 inhibitor on its own. Thus it was possible to obtain much smaller and more polar inhibitors, which exhibited up to 19-fold increased solubility. Furthermore, it became apparent that if a compound complies with the Ro5 plus contains a protonatable nitrogen, it is a good predictor for improved solubility.

As a side note it should be mentioned that in silico methods (we used the ACD/Structure Designer) failed to predict the solubility of our substances. Another common approach to estimate solubility is to use experimentally easily accessible parameters for guidance. For instance, the retention time in RP-HPLC analysis is linked to the lipophilicity of a compound [71] and the crystal lattice energy can be estimated from the melting point [2]. This approach turned out to be rather productive. For example, when comparing compound **49** with compound **1**, marked decreases in retention time (3.8 min vs. 7.2 min) and melting point (ca. 180 °C vs. 219 °C) were observed, in parallel with the increase in solubility (1.2 µM vs. 78 nM). Another operating experience worth disclosing is that adsorption of the substances to the vial surface can be critical. A case in point is compound **65**, which showed a 3-fold higher solubility when 'siliconized' PP vials (higher adsorption) were used instead of 'siliconized' glass vials (2.9 µM vs. 855 nM). Apparently, the presence of a layer of molecules adhering to the vial surface can influence the equilibrium in favor of higher solubility values.

Figure 12 summarizes the properties of the novel inhibitors that are most promising in terms of potency and solubility, specifically **40**, **41**, **48**, **49** and **65**, in comparison to our previous inhibitor **1** and fragment **27**. Depicted are IC_{50} values in the Hoechst 33342 assay and kinetic and thermodynamic solubility limits. As mentioned before, medicinal chemists often face the dilemma of improving solubility at the expense of diminished biological activity, due to the positive correlation of lipophilicity and affinity to hydrophobic binding pockets in drug targets [31]. The chart shows that by virtue of a fragment-based and rational approach we were able to circumvent this predicament and increase the equilibrium solubility of our compounds while maintaining inhibitory potency. Whereas compound **1** and fragment **27** exhibited equilibrium solubilities in the range of their potencies, the chromone inhibitors **40**, **41**, **48**, and **49** showed equilibrium solubilities that were three to nine times higher than their IC_{50} values. Compound **65**, the most soluble compound of the second series, showed an equilibrium solubility 2.5 times higher than its IC_{50} value.

As expected, the kinetic solubilities were considerably higher than the thermodynamic equilibrium solubilities. This means that by adding a DMSO stock solution to the buffer, a

supersaturated solution was produced in the concentration range between the thermodynamic and the kinetic solubility limit. Here it becomes obvious that time is a critical factor. On the time scale of the biological assays performed in this study, namely up to two hours, the precipitation of our previous inhibitor **1** was slow enough to allow for reliable results. However, since the thermodynamic (equilibrium) solubility of **1** was in the range of its IC_{50} value, compound **1** is not suited for in vitro assays requiring long time-periods of incubation and especially in vivo studies can be impaired. By contrast, the novel inhibitors with improved equilibrium solubility qualify for such examinations.

Lastly, there was no clear correlation between the thermodynamic and kinetic solubility, but as a tendency, higher kinetic solubility can be taken as a hint to increased equilibrium solubility.

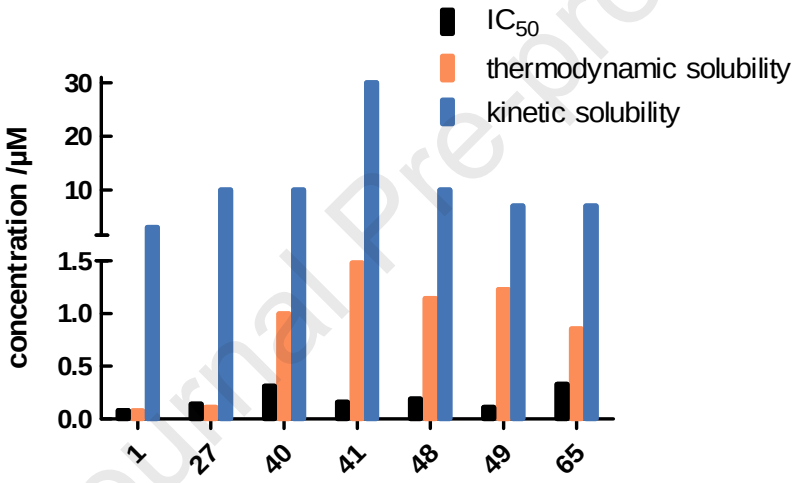

Figure 12. Comparison of the IC_{50} values in the Hoechst 33342 assay and kinetic and thermodynamic solubility limits of our previous tariquidar analog **1**, fragment **27**, the novel chromone inhibitors **40**, **41**, **48** and **49** as well as the novel, **1**-related inhibitor **65**.

3 Conclusion

Poor aqueous solubility has been reported to cause major problems with purification as well as in vitro and in vivo studies of biologically active compounds [3]. ABCG2 inhibitors are especially prone to solubility issues due to their size and lipophilic nature. Our previous, tariquidar-related inhibitor UR-MB108 (**1**) [28] shows high potency (79 nM), but extremely low equilibrium solubility (78 nM). This study comprises a solubility-driven discovery of novel ABCG2 inhibitors based on **1**. In a fragment-based approach, we synthesized and tested substructures of **1** for inhibitory potency, optimized them and included molecular docking experiments to grow the most promising fragments into inhibitors. The novel compounds inhibited ABCG2 with IC_{50} values in the two- to low three-digit nanomolar range, categorizing them among the most potent known ABCG2 inhibitors. Their ability to inhibit

ABCG2 transport was not only assessed in a Hoechst 33342 transport assay, but also confirmed by their ability to reverse the drug resistance in MCF7-Topo cells. The most promising compounds in terms of potency and solubility were the inhibitors UR-Ant116 (**40**), UR-Ant121 (**41**), UR-Ant131 (**48**) and UR-Ant132 (**49**), all of which displayed an *N*-phenyl-chromone-2-carboxamide scaffold. Their equilibrium solubility ranged between 1 µM and 1.5 µM, which puts them at the lower edge of the drug solubility window. Compared to **1**, this is an up to 19-fold improvement of equilibrium solubility. As a rule of thumb, the solubility of a potential drug should be at least three times its IC_{50} value. Compounds **40**, **41**, **48** and **49** exhibit solubilities of three to nine times their IC_{50} value – sufficient to exert their maximal effect. Moreover they do not or, in case of **40** only slightly, violate Lipinski's Ro5, which predicts good absorption properties in vivo. These four compounds differ in their biological profile. Whereas **41** was a triple ABCB1/ABCC1/ACBG2 inhibitor, compounds **42** and **49** were selective for ABCG2 and **48** was almost selective – it inhibited the other two subtypes only with very low potency and efficacy. Besides, the substances showed different modes of inhibition. An ATPase assay revealed that compounds **40** and **41** decreased the ATPase activity, whereas **48** and **49**, both differing structurally from the aforementioned two inhibitors, were partial ATPase activators. As a prerequisite for in vivo studies, we demonstrated the stability of the compounds in blood plasma and their non-toxicity.

Taken together, we offer scientists investigating ABCG2 a set of potent, selective and non-selective inhibitors that are stable, non-toxic and water-soluble (> 1 µM). To the best of our knowledge, this is the first study on ABCG2 inhibitors focusing on improved aqueous solubility and the first report providing not only biological, but also solubility information on the compounds. We expect them to be of great value for in vitro examinations requiring long time-periods of incubation such as structural biology studies on protein-ligand interactions using X-ray crystallography or NMR. Such studies depend on sufficient equilibrium solubility of the ligands; insufficient solubility has been identified as the cause of crystallography failures and as limitation to the method [72]. In the light of their stability in blood plasma and low toxicity, our substances are promising candidates for in vivo investigations, their aqueous solubility increasing the chances of success. For instance, due to their high selectivity, UR-Ant121 (**41**) and UR-Ant132 (**49**) should be well-suited as pharmacological tools for PET studies of ABCG2, e.g. at the BBB, provided that appropriate radioactive labeling can be achieved. Up to now, inhibitors of ABCG2 are not in clinical use yet [73]. Potential therapeutic applications were explored in several in vivo studies [73,74], for instance as a means to overcome the BBB and MDR. Since ABCB1 and ABCG2 (and to a lesser extent

ABCC1) act in concert at many physiological barriers [75], the triple ABCB1/ABCC1/ABCG2 inhibitor UR-Ant116 (**40**) is an attractive candidate for therapeutic studies.

4 Experimental Section

4.1 Chemistry

4.1.1 General Experimental Conditions

Chemicals and solvents were purchased from commercial suppliers (Sigma Aldrich, Munich, Germany; Merck, Darmstadt, Germany; VWR, Darmstadt, Germany; Thermo Fisher Scientific, Waltham, MA, USA; TCI, Eschborn, Germany) and used without further purification unless stated otherwise. Reactions requiring anhydrous conditions were carried out in dry reaction vessels under an atmosphere of argon and anhydrous solvents were used. Millipore water was used throughout for the preparation of buffers and HPLC eluents. Acetonitrile for HPLC (gradient grade) was obtained from Merck.

Microwave reactions were carried out in an Initiator 8 microwave reactor (Biotage, Uppsala, Sweden).

Thin layer chromatography was performed on TLC Silica gel 60 F_{254} aluminium plates (Merck, Darmstadt, Germany). Visualization was accomplished by UV irradiation at wavelengths of 254 nm and 366 nm or by staining with ninhydrin (1.5 g ninhydrin, 5 mL acetic acid, 500 mL 95% ethanol).

For **column chromatography** Geduran® Silica 60 gel (0.040-0.063 mm; Merck, Darmstadt, Germany) was used.

Automated flash column chromatography was performed on a 971-FP Flash Purification System (Agilent Technologies, Santa Clara, CA, USA) using pre-packed SuperFlash Silica 50 columns (Agilent Technologies). The crude products were dissolved in a suitable solvent, mixed with Geduran® Silica 60 gel (0.040-0.063 mm; Merck, Darmstadt, Germany), concentrated under reduced pressure and placed in a load cartridge prior to the run.

Melting points were determined with a Büchi B-540 apparatus (Büchi Labortechnik, Essen, Germany) and are uncorrected.

NMR spectra were recorded on an Avance 300 instrument (7.05 T, ^{1}H: 300.1 MHz, ^{13}C: 75.5 MHz), an Avance 400 instrument (9.40 T, ^{1}H: 400 MHz, ^{13}C: 101 MHz) or an Avance 600 instrument with cryogenic probe (14.1 T, ^{1}H: 600 MHz, ^{13}C: 151 MHz) (Bruker, Karlsruhe, Germany) with TMS as external standard.

High-resolution mass spectrometry (HRMS) analysis was performed on an Agilent 6540 UHD Accurate-Mass Q-TOF LC/MS system (Agilent Technologies, Santa Clara, CA, USA) using an ESI source.

Low-resolution mass spectrometry (MS) was performed on a Finnigan MAT SSQ 710 A GC/MS system (Finnigan MAT, now Thermo Fisher Scientific, Waltham, MA, USA).

Preparative HPLC was performed on a system from Knauer (Berlin, Germany) consisting of two K-1800 pumps and a K-2001 detector. A Kinetex® XB-C18 (5 µm, 100 Å, 250 mm x 21.2 mm; Phenomenex, Aschaffenburg, Germany) served as RP-column at a flow-rate of 15 mL/min. Mixtures of acetonitrile and 0.1% aq TFA were used as mobile phase. The detection wavelength was set to 220 nm throughout. The solvent mixtures were removed by lyophilisation using an Alpha 2-4 LD lyophilisation apparatus (Christ, Osterode am Harz, Germany) equipped with an RZ 6 rotary vane vacuum pump (Vacuubrand, Wertheim, Germany).

Analytical HPLC was performed on a system from Agilent Technologies (Santa Clara, CA, USA) (Series 1100) composed of a G1312A binary pump equipped with a G1379A degasser, a G1329A ALS autosampler, a G1316A COLCOM thermostated column compartment and a G1314A VWD detector. A Kinetex® C8 (2.6 µm, 100 Å, 100 mm × 4.6 mm; Phenomenex, Aschaffenburg, Germany) served as RP-column at a flow rate of 1 mL/min. Oven temperature was set to 30 °C throughout. Mixtures of acetonitrile (A) and 0.05% aq TFA (B) were used as mobile phase. The detection wavelength was set to 220 nm throughout. Solutions for injection (40 µM) were prepared by diluting a stock solution in DMSO with a mixture of A and B corresponding to the composition of the eluent at the start of the gradient. The following linear gradient was applied: 0-12 min: A/B 30:70-95:5, 12-15 min: A/B 95:5. Retention (capacity) factors were calculated from retention times (t_R) according to $k = (t_R - t_0)/t_0$ (t_0 = dead time).

X-Ray analysis. Single clear colorless prism-shaped crystals of compound **4** were obtained by recrystallization from $CHCl_3$. A crystal (0.35×0.21×0.20) was selected and mounted on a MITIGEN holder oil on a SuperNova, Single source at offset, Atlas diffractometer. The crystal was kept at T = 123.00(10) K during data collection. Using Olex2 (Dolomanov et al., 2009), the structure was solved with the ShelXT (Sheldrick, 2015) structure solution program, using the Direct Methods solution method. The model was refined with olex2.refine (Bourhis et al., 2015) using Gauss-Newton minimization.

4.1.2 Synthesis Protocols and Analytical Data

The synthesis procedures for the intermediate and the final compounds as well as the appertaining analytical data can be found in the Supporting Information. All compounds were characterized by ^{1}H and ^{13}C NMR spectroscopy, (HR)MS, and melting point (if applicable). In addition, final compounds were characterized by RP-HPLC (purity control). The purity of the final compounds was ≥ 95% throughout.

4.2 Molecular Docking

ABCG2 transporter and ligand preparation. The cryo-EM structure of the human ABCG2 transporter (PDB ID: 5NJ3 [30]) was used as template. To reconstitute missing N-termini and loops, Modeller 9.18 [76-78] was used. The ABCG2 model contained disulfide bridges within each monomer (Cys592 - Cys608) and between the monomers (Cys603 - Cys603). Coordinates of the antibody 5D3-Fab were removed. Protein and ligand preparation (Schrödinger LLC, Portland, OR, USA) including an assignment of protonation states were essentially performed as described [79,80] before. Compounds **27**, **48** and **50** were considered in the unprotonated state.

Induced-fit docking. Compounds **27**, **48**, **50** and further potential ligands were docked "flexibly" to the ABCG2 transporter using the induced-fit docking module (Schrödinger LLC). The ligands were docked within a box of 46 × 46 × 46 $Å^3$ around the center of mass between N436 of the first and the second monomer, respectively. Redocking was performed in the extended precision mode. From the induced-fit docking results obtained, one pose (ligand-ABCG2 transporter complex) was selected based on low/minimal XP Gscores and reasonability of the ligand binding pose. Ligand-receptor interactions were analyzed using PLIP 1.4.2 [81]. Figures showing molecular structures of the ABCG2 transporter in complex with **27** or **48** were generated with PyMOL Molecular Graphics system, version 2.2.0 (Schrödinger LLC).

4.3 Biological Assays

4.3.1 General Experimental Conditions

Materials. Commodity chemicals and solvents were purchased from commercial suppliers (Sigma Aldrich, Munich, Germany; Merck, Darmstadt, Germany; VWR, Darmstadt, Germany; Thermo Fisher Scientific, Waltham, MA, USA; Invitrogen, Karlsruhe, Germany). Topotecan and vinblastine were obtained from Sigma Aldrich. Hoechst 33342 and calcein-AM were procured from Biotium (Fremont, CA, USA). FTC was from Merck. Tariquidar was synthesized in our laboratory according to literature [82] with slight modifications [83].

Reversan was obtained from Tocris (Wiesbaden-Nordenstadt, Germany). Millipore water was used throughout for the preparation of buffers, aqueous reagent solutions and HPLC eluents. The pH of buffers and aqueous reagent solutions was adjusted with NaOH aq or HCl aq unless stated otherwise. Acetonitrile for HPLC (gradient grade) was obtained from Merck. All cell lines were purchased from the ATCC (American Type Culture Collection; Manassas, VA, USA). Tissue culture flasks were procured from Sarstedt (Nümbrecht, Germany). Dulbecco's Modified Eagle's Medium - high glucose (DMEM/High; with 4500 mg/L glucose, sodium pyruvate and sodium bicarbonate, without L-glutamine, liquid, sterile-filtered, suitable for cell culture) and L-glutamine solution (200 mM, sterile-filtered, BioXtra, suitable for cell culture) were from Sigma Aldrich. Fetal calf serum (FCS) and trypsin/EDTA and were from Biochrom (Berlin, Germany). For all assays in microplate format, 96-well plates (PS, clear, F-bottom, with lid, sterile) from Greiner Bio-One (Frickenhausen, Germany) were used. Human CPD (citrate, phosphate, dextrose) plasma was a gift from the Bavarian Red Cross (Regensburg, Germany). Syringe filters (Phenex-RC, 4 mm, 0.2 µm) used in the chemical stability assay (in blood plasma) were from Phenomenex (Aschaffenburg, Germany).

Stock solutions. Topotecan and vinblastine were dissolved in 70% EtOH to give 100 µM stock solutions. Hoechst 33342 stock solution (0.8 mM) was prepared in water and calcein-AM stock solution (100 µM) in DMSO. The test compounds and the reference compounds fumitremorgin C, tariquidar, reversan and sulfasalazine were dissolved in DMSO at 100 times the final concentrations in the transport assays and the ATPase assay and at 1000 times the final concentrations in the chemosensitivity assay. For the stability assay in blood plasma, 10 mM stock solutions of the test compounds were prepared in DMSO. If not stated otherwise, millipore water served as solvent for other assay reagents.

Instruments. Fluorescence and absorbance measurements in microplates were carried out with a GENios Pro microplate reader (equipped with a Xenon arc lamp; Tecan, Grödig, Austria). Analytical HPLC after incubation in human blood plasma was performed on a system from Agilent described above (chemistry – general experimental conditions). The HPLC conditions were as described, yet with two alterations. The following linear gradient was applied: 0-12 min: A/B 20:80-95:5, 12-15 min: A/B 95:5. The injection volume was 100 µL.

Software. All biological data were analyzed with GraphPad Prism 5 (GraphPad Software, San Diego, CA, USA).

4.3.2 Cell Culture

All cells were cultured in DMEM/High supplemented with 2% (v/v) of a 200 mM L-glutamine solution and 10% (v/v) FCS at 37 °C in a water-saturated atmosphere containing 5% CO_2.

MCF-7/Topo cells, an ABCG2-overexpressing variant of the MCF-7 cell line (ATCC® HTB-22), were obtained by passaging the MCF-7 cells with increasing amounts of topotecan in the culture medium to achieve a maximum concentration of 550 nM within a period of about 40 d; after 3 passages at the maximum concentration the treated cells expressed sufficient quantities of ABCG2 [84,85]. Cells were cultured in the presence of topotecan (550 nM) to maintain overexpression of the ABCG2 transporter.

KB-V1 cells, an ABCB1-overexpressing variant of the KB cell line (ATCC® CCL-17), were obtained by passaging the KB cells with increasing amounts of vinblastine in the culture medium to achieve a maximum concentration of 330 nM within a period of about 90 d; after 3 passages at the maximum concentration the treated cells expressed sufficient quantities of ABCB1 transporter [83,86]. They were cultured with 330 nM vinblastine to maintain overexpression of the ABCB1 transporter.

MDCK.2-MRP1 cells were a kind gift from Prof. Dr. P. Borst from the Netherland Cancer Institute (Amsterdam, NL). They were obtained by transfecting MDCK.2 cells (ATCC® CRL-2936) with human ABCC1 [87,88]. Due to the strong adherence of this cell line, trypsinization was performed using 2X trypsin/EDTA (0.1%./0.04%) for 30 min.

All cells were routinely monitored for mycoplasma contamination by PCR using the Venor®GeM mycoplasma detection kit (Minerva Biolabs, Berlin, Germany) and were negative.

4.3.3 Inhibition of ABCG2: Hoechst 33342 Transport Assay

The assay was performed as described in our previous report [28], applying the following modification: cells were seeded into 96-well plates at a density of 18,000 cells per well (instead of 20,000).

4.3.4 Inhibition of ABCB1: Calcein-AM Transport Assay

The assay was performed as described in our previous report [28].

4.3.5 Inhibition of ABCC1: Calcein-AM Transport Assay

The assay was performed as described in our previous report [28].

4.3.6 Chemosensitivity Assay

The assay was performed as described in our previous report [28].

Cytotoxic effects were expressed as corrected T/C-values according to

$$T / C_{corr}[\%] = \frac{T - C_0}{C - C_0} \cdot 100$$

where T is the mean absorbance of the treated cells, C the mean absorbance of the negative controls and C_0 the mean absorbance of the cells at the time of compound addition (t_0). When the absorbance of treated cells T was lower than at the beginning of the experiment (C_0), the extent of cell killing was calculated as cytocidal effect according to

$$Cytocidal \quad effect \quad [\%] = \frac{T - C_0}{C_0} \cdot 100$$

4.3.7 ABCG2 ATPase Assay

Membrane preparation. The protocol is based on the procedure of Sarkadi et al. [89] and our previous report [28]. MCF-7/Topo cells were harvested after trypsinization by centrifugation at 4 °C and 500 g for 10 min. The cell pellet was re-suspended in Tris mannitol buffer (50 mM Tris, 300 mM mannitol, 0.5 mM phenylmethylsulfonyl fluoride (PMSF), pH 7; 100 mL) and centrifuged again. Then the pellet was lysed and homogenized in TMEP buffer (50 mM Tris, 50 mM mannitol, 1 mM EDTA, 10 µg/mL leupeptin, 10 µg/mL benzamidine, 0.5 mM PMSF, 2 mM DTT, pH 7; 60 mL) by a Potter Elvehjem tissue homogenizer. Undisrupted cells and cellular debris were pelleted by centrifugation at 4 °C and 500 g for 10 min and the supernatant, containing the membranes, was removed carefully. After centrifugation at 4 °C and 100,000 g for 1 h the pellet (containing the membranes) was re-suspended in TMEP buffer (30 mL), giving a protein concentration of 2.0-3.0 mg/mL, and homogenized with a Potter Elvehjem tissue homogenizer. All procedures during the membrane preparation were performed at 4 °C and aliquots (500-1000 µL) were stored at -80 °C until use.

Protein quantification was performed by the method of Bradford using the Bio-Rad protein assay kit according to the manual.

Assay procedure. The assay was performed by analogy with the ABCB1 ATPase assay procedure described by Sarkadi et al. [89] and the procedure described in our previous report [28]. The ATPase activity of the ABCG2 transporter was estimated by measuring inorganic phosphate liberation. It was determined as orthovanadate-sensitive ATPase activity in the presence of inhibitors in ABCG2 MCF-7/Topo membrane preparations.

Membranes containing 2.0-2.5 mg of total soluble protein were thawed on ice and pelleted by centrifugation at 4 °C and 16,200 g for 10 min. Then they were suspended in assay buffer (50 mM MOPS-Tris (100 mM MOPS, pH adjusted to 7.0 with 1.7 M Tris), 50 mM KCl,

5 mM NaN_3, 2 mM EGTA, 2 mM DTT, 1 mM ouabain; 4.2 mL), mixed with 10% (w/w) CHAPS (42 µL; decreases the high basal ABCG2 ATPase activity) and homogenized using a syringe and a needle (27G). The suspension was split into 2 portions (2.0 mL each) and one portion was supplemented with orthovanadate (100 mM Na_3VO_4, pH 10; 50 µL; final conc. 2 mM), the other with the same amount of purified water. The two suspensions (w. and wo. orthovanadate) were transferred into a 96-well plate on ice (40 µL/well; 20-25 µg protein/well) and pre-incubated at 37 °C for 3 min.

The ATPase reaction was started by adding the reference and test compounds in assay buffer containing 20 mM ATP (10 µL/well, giving a final volume of 50 µL/well; final conc. 4 mM) with a multichannel pipette and the plate was incubated at 37 °C in a microplate shaker for 1 h. For this purpose, an ATP solution (200 mM Mg_xATP, 400 mM $MgCl_2$, pH adjusted to 7.0 with 1.7 M Tris) was diluted 1:10 (v/v) with assay buffer and the test and reference compounds were added 5-fold concentrated. Sulfasalazine at a final concentration of 30 µM served as reference activator (positive control); the vehicle DMSO (1% final content) served as negative control. Each concentration (w. and wo. orthovanadate) was measured in duplicate, positive and negative control in quadruplicate each.

The reaction was stopped by the addition of 10% (w/w) SDS (30 µL/well); background control (phosphate stemming from the assay buffer) (w. and wo. orthovanadate) was stopped before starting the reaction with MgATP and was measured in duplicate.

Phosphate standards (0, 0.05, 0.1, 0.25, 1.5 and 2.0 mM NaH_2PO_4 in assay buffer; 50 µL/well; each concentration measured in duplicate) were included on each plate for calibration.

The amount of phosphate was determined by adding a colorimetric reagent (1 part of reagent A (35 mM ammonium molybdate, 15 mM zinc acetate) mixed with 4 parts of reagent B (5% (w/w) ascorbic acid, pH 5.0; freshly prepared); 200 µL/well) and by incubating at 37 °C for further 20 min. The absorbance (820 nm) as a parameter proportional to the phosphate amount was measured, using a GENios Pro microplate reader.

The data obtained under the treatment with orthovanadate were subtracted from the data without orthovanadate to obtain phosphate liberation resulting from ABCG2 activity. The ensuing data were normalized relative to the absorbance in the absence of an ABCG2 activator (negative control) and the response elicited by the sulfasalazine (positive) control, which was defined as 100% ATPase activity. IC_{50} values were calculated using four parameter sigmoidal fits. Errors were expressed as standard error of the mean (SEM).

4.3.8 Chemical Stability Assay (in Blood Plasma)

The human CPD (citrate, phosphate, dextrose) blood plasma samples were stored at - 80 °C and thawed before use. Stock solutions of the test compounds (10 mM in DMSO) were diluted 1:50 with blood plasma, giving a concentration of 200 µM. The samples were vortexed briefly and incubated at 37 °C. After different periods of time, aliquots were taken and deproteinated by adding three parts of ice-cold MeCN, vortexing and storing at 4 °C for 30 min. Samples were centrifuged at 4 °C and 16,000 g for 5 min and the supernatants were diluted 1:1 with 0.05% TFA aq and stored at - 80 °C until analyzed. They were thawed at room temperature, filtered with syringe filters and analyzed with HPLC.

4.4 Solubility Assays

4.4.1 General Experimental Conditions

Materials. Chemicals and solvents were purchased from commercial suppliers (Sigma Aldrich, Munich, Germany; Merck, Darmstadt, Germany; VWR, Darmstadt, Germany; Thermo Fisher Scientific, Waltham, MA, USA). Millipore water was used throughout for the preparation of buffers and HPLC eluents. The pH of buffers was adjusted with NaOH aq and HCl aq. Buffers were filtered before use. Acetonitrile for HPLC (gradient grade) was obtained from Merck. Micro tubes were from Sarstedt (Nümbrecht, Germany). 96-Well plates (PS, clear, F-bottom, with lid, sterile) were acquired from Greiner Bio-One (Frickenhausen, Germany). Glass vials (with PE plug) were procured from Altmann Analytik (München, Germany); borosilicate glass centrifuge tubes (without plug) from Thermo Fisher Scientific. Sigmacote® (Sigma Aldrich) was used as siliconizing agent for the vials. Parafilm (Bemis, Neenah, WI, USA) was used to cap the centrifuge tubes.

Stock solutions. The test compounds and the reference compound haloperidol were dissolved in DMSO at 1000 times the final concentrations in the thermodynamic solubility assay and for the calibration curve at 100 times the final concentrations. Furthermore, the test compounds and the reference compound coronene were dissolved at 100 times the final concentrations in the kinetic solubility assay.

Instruments. For incubating and shaking vials an MB-102 ThermoCell mixing block (BIOER, Hangzhou, China) was used. Analytical HPLC of the samples from the thermodynamic solubility assay was performed on a system from Agilent, described above (chemistry – general experimental conditions). The HPLC conditions were as described with two alterations. The following linear gradient was applied: 0-8 min: A/B 30:70-73:27, 8-9 min: A/B 73:27-95:5, 9-12 min: A/B 95:5, 12-13 min: A/B 95:5-30:70. The injection

volume was 100 µL. Absorbance measurements of the microplates were carried out with a GENios Pro microplate reader (Tecan, Männedorf, Switzerland).

Software. Data were analyzed with Microsoft Excel and GraphPad Prism 5 (GraphPad Software, San Diego, CA, USA). ClogP values were calculated with ACD/Structure Designer, version 12 (Advanced Chemistry Development, Inc. (ACD/Labs), Toronto, Canada).

4.4.2 Kinetic Solubility Assay

UV-VIS Spectra of the test compounds were recorded along with the high-resolution mass spectrometry (HRMS) analysis, which was performed on the Agilent LC/MS system described above (chemistry – general experimental conditions); the system was additionally equipped with a 1290 DAD detector (Agilent Technologies, Santa Clara, CA, USA).

Assay Procedure. The kinetic solubility was determined turbidimetrically. DMSO stock solutions of the test compound (different concentrations) were diluted 1:100 with the respective buffer (pH 7.4) at 37 °C in a micro tube (10 µL stock in 1000 µL buffer), giving a final DMSO concentration of 1%. The sample was vortexed and transferred into a 96-well plate (300 µL/well, 3 replicate wells). DMSO (1% in buffer; 300 µL/well, measured 12-fold) served as vehicle control/ blank value, coronene served as a highly insoluble control compound. After incubating the plate at 37 °C for 2 h, the extinction was measured at 380 nm using a GENios Pro microplate reader. The data were normalized to the blank value and the kinetic solubility limit was estimated as the highest concentration at which more than 95% of the radiation is transmitted (i.e. the extinction is lower than 0.0223).

4.4.3 Thermodynamic Solubility Assay

The thermodynamic solubility of the test and reference compounds was determined by the saturation shake-flask method. A DMSO stock solution of the test compound was diluted 1:1000 in PBS (pH 7.4) in a glass vial or glass centrifuge tube, both of which had been treated with a siliconizing agent, giving a final DMSO content of 1‰ (e.g. 0.6 µL stock in 600 µL PBS). According to solubility, stock solutions of different concentrations were used (compounds **40**, **41**, **48** and **49**: 50 mM, compound **65**: 20 mM, all other compounds: 10 mM). The vial was capped, vortexed and shaken at 25 °C for 36-40 h. Shaking was stopped and the precipitate was allowed to sediment at 25 °C for 24 h. In the case of poorly sedimenting compounds, the samples were then centrifuged at 25 °C and 2700 g for 30 min. 2 aliquots of supernatant (100 µL each) were taken carefully from each vial with a micropipette, anxious not to swirl up the sediment, and diluted with MeCN (50 µL). The micropipette tip was rinsed thoroughly in the mixture of supernatant and MeCN to dissolve potential residue adsorbed to the tip surface. The sample was analyzed with HPLC and the peak area was determined.

Standard solutions were produced as follows. DMSO stock solutions (5 concentrations) and DMSO were diluted 1:100 in PBS (1% final DMSO content), vortexed and immediately an aliquot (100 µL) from each solution was taken and diluted with MeCN (50 µL) (plus pipette tip was rinsed). The standards were measured by HPLC and the peak areas were used to construct a calibration curve. Solubility of the test compound was determined by quantifying the concentration of the sample using the calibration curve. At least 6 independent experiments were carried out for each reported result. Errors were expressed as standard error of the mean (SEM).

Author Information

Corresponding Author

* E-mail: frauke.antoni@ur.de. Phone: (+49)941-943-2925. Fax: (+49)941-943-4820.

ORCID

Frauke Antoni: 0000-0001-8382-6315

David Wifling: 0000-0002-1370-2138

Günther Bernhardt: 0000-0001-6491-9874

Present Address

[#]Leibniz Supercomputing Centre of the Bavarian Academy of Sciences and Humanities, Boltzmannstraße 1, 85748 Garching, Germany.

Author Contributions

F.A. conceived the project with input from the co-authors. F.A. designed the target structures; **48**, **49** and **50** were designed by F.A. and D.W. together. D.W. performed the molecular docking studies. F.A. performed the synthesis, the biological assays, the solubility assays and the data analysis with G.B. as a supervisor. F.A. wrote the manuscript with input from all co-authors.

Declaration of Competing Interest

The authors declare that they have no known competing financial interests or personal relationships that could have appeared to influence the work reported in this paper.

Acknowledgements

The authors thank Lydia Schneider and Maria Beer-Krön for excellent technical assistance, Marlies Antoni for skillful linguistic support, Michael Thormann (Origenis GmbH, München, Germany) for helpful discussions, and the Leibniz Supercomputing Centre (LRZ) in Munich for providing software (Schrödinger suite) and computing resources.

Appendix. Supplementary data

The Supporting Information contains the Figures S1 and S2, the synthesis procedures and analytical data of all intermediate and final compounds as well as ^{1}H and ^{13}C NMR spectra and RP-HPLC analysis (purity control) of the final compounds.

Abbreviations

ABC, ATP-binding cassette transporter; ABCB1, ATP-binding cassette transporter, subfamily B, member 1; ABCC1, ATP-binding cassette transporter, subfamily C, member 1; ABCG2, ATP-binding cassette transporter, subfamily G, member 2; ADME-Tox, absorption, distribution, metabolism, excretion and toxicity; ADP, adenosine diphosphate; ATP, adenosine triphosphate; BBB, blood-brain barrier; BCRP, breast cancer resistance protein; Calcein-AM, calcein acetoxymethyl ester; CHAPS, 3-((3-cholamidopropyl)dimethylammonio)-1-propanesulfonate; clogP, calculated logP value; cryo-EM, cryogenic electron microscopy; CuAAC, copper-catalyzed azide-alkyne cycloaddition; DCM, dichloromethane; DIPEA, *N*,*N*-diisopropylethylamine; DMEM, Dulbecco's modified Eagle's medium; DMF, dimethyformamide; DMSO, dimethylsulfoxide; DTT, dithiothreitol; EDTA, ethylenediaminetetraacetic acid; EtOH, ethanol; FCS, fetal calf serum; FTC, fumitremorgin C; GBB, gut-blood barrier; HPLC, high-pressure liquid chromatography; HRMS, high-resolution mass spectrometry; IC_{50}, concentration of inhibitor required to give 50% inhibition of activity; mAU, milli-absorbance units; MDR, multidrug resistance; MeCN, acetonitrile; MeOH, methanol; MRP1, multidrug resistance associated protein 1; MS, (low resolution) mass spectrometry; MWT, molecular weight; NMR, nuclear magnetic resonance; NMRI, Naval Medical Research Institute; PBS, phosphate buffered saline; PCR, polymerase chain reaction; Pd/C, palladium on activated charcoal; PET, positron emission tomography; PMSF, phenylmethylsulfonyl fluoride; PP, polypropylene; Ro5, rule of five; RP-HPLC, reversed-phase high-pressure liquid chromatography; SDS, sodium dodecyl sulfate; SEM, standard error of the mean; TBTA, tris((1-benzyl-4-triazolyl)methyl)amine; TBTU, 2-(1*H*-Benzotriazole-1-yl)-1,1,3,3-tetramethylaminium tetrafluoroborate; TFA, trifluoroacetic acid;

THF, tetrahydrofuran; TLC, thin layer chromatography; TMEP, Tris, mannitol, EDTA, leupeptin, benzamidine, PMSF, DTT (buffer ingredients); TMS, trimethylsilyl; Tris, tris(hydroxymethyl)aminomethane; UV, ultraviolet; VIS, visible.

References

[1] C.A. Lipinski, F. Lombardo, B.W. Dominy, P.J. Feeney, Experimental and computational approaches to estimate solubility and permeability in drug discovery and development settings, Adv. Drug Delivery Rev., 23 (1997) 3-25.
[2] C. Lipinski, Drug Solubility in Water and Dimethylsulfoxide, in: R. Mannhold, H. Kubinyi, G. Folkers (Eds.) Molecular Drug Properties, Wiley-VCH, Weinheim, Germany, 2008, pp. 255-282.
[3] L. Di, P.V. Fish, T. Mano, Bridging solubility between drug discovery and development, Drug Discov. Today, 17 (2012) 486-495.
[4] R.J. Young, Physical Properties in Drug Design, in: N.A. Meanwell (Ed.) Tactics in Contemporary Drug Design, Springer, 2015, pp. 1-68.
[5] A.M. Davis, S.J. Teague, Hydrogen Bonding, Hydrophobic Interactions, and Failure of the Rigid Receptor Hypothesis, Angew. Chem., Int. Ed., 38 (1999) 736-749.
[6] Z. Guo, B. Li, L.-T. Cheng, S. Zhou, J.A. McCammon, J. Che, Identification of Protein–Ligand Binding Sites by the Level-Set Variational Implicit-Solvent Approach, J. Chem. Theory Comput., 11 (2015) 753-765.
[7] L. Zhang, H. Zhu, A. Mathiowetz, H. Gao, Deep understanding of structure–solubility relationship for a diverse set of organic compounds using matched molecular pairs, Bioorg. Med. Chem., 19 (2011) 5763-5770.
[8] S.N. Bhattachar, L.A. Deschenes, J.A. Wesley, Solubility: it's not just for physical chemists, Drug Discov. Today, 11 (2006) 1012-1018.
[9] B. Faller, P. Ertl, Computational approaches to determine drug solubility, Adv. Drug Delivery Rev., 59 (2007) 533-545.
[10] K.T. Savjani, A.K. Gajjar, J.K. Savjani, Drug solubility: importance and enhancement techniques, ISRN Pharm., 2012 (2012) 195727-195727.
[11] S.H. Yalkowsky, J.F. Krzyzaniak, G.H. Ward, Formulation-Related Problems Associated with Intravenous Drug Delivery, J. Pharm. Sci., 87 (1998) 787-796.
[12] L. Di, E.H. Kerns, G.T. Carter, Drug-like property concepts in pharmaceutical design, Curr. Pharm. Des., 15 (2009) 2184-2194.
[13] N.M. Ahmad, Solubility-driven lead optimisation: Recent examples and personal perspectives, Bioorg. Med. Chem. Lett., 26 (2016) 2975-2979.
[14] M. Ishikawa, Y. Hashimoto, Improvement in Aqueous Solubility in Small Molecule Drug Discovery Programs by Disruption of Molecular Planarity and Symmetry, J. Med. Chem., 54 (2011) 1539-1554.
[15] M.A. Walker, Improving Solubility via Structural Modification, in: N.A. Meanwell (Ed.) Tactics in Contemporary Drug Design, Springer, Berlin, Heidelberg, 2015, pp. 69-106.
[16] S. Höfinger, F. Zerbetto, On the Cavitation Energy of Water, Chem. – Eur. J., 9 (2003) 566-569.
[17] L. Gandhi, D.R. Camidge, M. Ribeiro de Oliveira, P. Bonomi, D. Gandara, D. Khaira, C.L. Hann, E.M. McKeegan, E. Litvinovich, P.M. Hemken, C. Dive, S.H. Enschede, C. Nolan, Y.-L. Chiu, T. Busman, H. Xiong, A.P. Krivoshik, R. Humerickhouse, G.I. Shapiro, C.M. Rudin, Phase I study of Navitoclax (ABT-263), a novel Bcl-2 family inhibitor, in patients with small-cell lung cancer and other solid tumors, J. Clin. Oncol., 29 (2011) 909-916.

[18] C.A. Lipinski, Rule of five in 2015 and beyond: Target and ligand structural limitations, ligand chemistry structure and drug discovery project decisions, Adv. Drug Delivery Rev., 101 (2016) 34-41.
[19] D.A. DeGoey, H.-J. Chen, P.B. Cox, M.D. Wendt, Beyond the Rule of 5: Lessons Learned from AbbVie's Drugs and Compound Collection, J. Med. Chem., 61 (2018) 2636-2651.
[20] Bradley C. Doak, B. Over, F. Giordanetto, J. Kihlberg, Oral Druggable Space beyond the Rule of 5: Insights from Drugs and Clinical Candidates, Chem. Biol., 21 (2014) 1115-1142.
[21] A. Klamt, B.J. Smith, Challenge of Drug Solubility Prediction, in: R. Mannhold, H. Kubinyi, G. Folkers (Eds.) Molecular Drug Properties, Wiley-VCH, Weinheim, Germany, 2008, pp. 283-311.
[22] B.E. Blass, In vitro ADME and In vivo Pharmacokinetics, in: B.E. Blass (Ed.) Basic Principles of Drug Discovery and Development, Academic Press, Boston, 2015, pp. 245-306.
[23] L.A. Doyle, W. Yang, L.V. Abruzzo, T. Krogmann, Y. Gao, A.K. Rishi, D.D. Ross, A multidrug resistance transporter from human MCF-7 breast cancer cells, Proc. Natl. Acad. Sci. U. S. A., 96 (1999) 2569.
[24] E. Rocchi, A. Khodjakov, E.L. Volk, C.-H. Yang, T. Litman, S.E. Bates, E. Schneider, The Product of the ABC Half-Transporter Gene ABCG2 (BCRP/MXR/ABCP) Is Expressed in the Plasma Membrane, Biochem. Biophys. Res. Commun., 271 (2000) 42-46.
[25] A. Mahringer, G. Fricker, ABC transporters at the blood-brain barrier, Expert Opin. Drug Metab. Toxicol., 12 (2016) 499-508.
[26] B.C. Baguley, Multiple Drug Resistance Mechanisms in Cancer, Mol. Biotechnol., 46 (2010) 308-316.
[27] A. Spindler, K. Stefan, M. Wiese, Synthesis and Investigation of Tetrahydro-β-carboline Derivatives as Inhibitors of the Breast Cancer Resistance Protein (ABCG2), J. Med. Chem., 59 (2016) 6121-6135.
[28] F. Antoni, M. Bause, M. Scholler, S. Bauer, S.A. Stark, S.M. Jackson, I. Manolaridis, K.P. Locher, B. König, A. Buschauer, G. Bernhardt, Tariquidar-related triazoles as potent, selective and stable inhibitors of ABCG2 (BCRP), Eur. J. Med. Chem., 191 (2020) 112133.
[29] S.M. Jackson, I. Manolaridis, J. Kowal, M. Zechner, N.M.I. Taylor, M. Bause, S. Bauer, R. Bartholomaeus, G. Bernhardt, B. Koenig, A. Buschauer, H. Stahlberg, K.-H. Altmann, K.P. Locher, Structural basis of small-molecule inhibition of human multidrug transporter ABCG2, Nat. Struct. Mol. Biol., 25 (2018) 333-340.
[30] N.M.I. Taylor, I. Manolaridis, S.M. Jackson, J. Kowal, H. Stahlberg, K.P. Locher, Structure of the human multidrug transporter ABCG2, Nature, 546 (2017) 504-509.
[31] G.G. Ferenczy, G.M. Keserű, Enthalpic Efficiency of Ligand Binding, J. Chem. Inf. Model., 50 (2010) 1536-1541.
[32] G.G. Ferenczy, G.M. Keserű, On the enthalpic preference of fragment binding, MedChemComm, 7 (2016) 332-337.
[33] A. Bancet, C. Raingeval, T. Lomberget, M. Le Borgne, J.-F. Guichou, I. Krimm, Fragment Linking Strategies for Structure-Based Drug Design, J. Med. Chem., (2020).
[34] H.C. Kolb, M.G. Finn, K.B. Sharpless, Click Chemistry: Diverse Chemical Function from a Few Good Reactions, Angew. Chem., Int. Ed., 40 (2001) 2004-2021.
[35] S. Bauer, C. Ochoa-Puentes, Q. Sun, M. Bause, G. Bernhardt, B. Koenig, A. Buschauer, Quinoline Carboxamide-Type ABCG2 Modulators: Indole and Quinoline Moieties as Anilide Replacements, ChemMedChem, 8 (2013) 1773-1778.
[36] S.C. Köhler, M. Wiese, HM30181 Derivatives as Novel Potent and Selective Inhibitors of the Breast Cancer Resistance Protein (BCRP/ABCG2), J. Med. Chem., 58 (2015) 3910-3921.

[37] D. Peña-Solórzano, M. Scholler, G. Bernhardt, A. Buschauer, B. König, C. Ochoa-Puentes, Tariquidar-Related Chalcones and Ketones as ABCG2 Modulators, ACS Med. Chem. Lett., 9 (2018) 854-859.
[38] G.J. Gozzi, Z. Bouaziz, E. Winter, N. Daflon-Yunes, D. Aichele, A. Nacereddine, C. Marminon, G. Valdameri, W. Zeinyeh, A. Bollacke, J. Guillon, A. Lacoudre, N. Pinaud, S.M. Cadena, J. Jose, M. Le Borgne, A. Di Pietro, Converting Potent Indeno[1,2-b]indole Inhibitors of Protein Kinase CK2 into Selective Inhibitors of the Breast Cancer Resistance Protein ABCG2, J. Med. Chem., 58 (2015) 265-277.
[39] G.J. Gozzi, Z. Bouaziz, E. Winter, N. Daflon-Yunes, M. Honorat, N. Guragossian, C. Marminon, G. Valdameri, A. Bollacke, J. Guillon, N. Pinaud, M. Marchivie, S.M. Cadena, J. Jose, M. Le Borgne, A. Di Pietro, Phenolic indeno[1,2-b]indoles as ABCG2-selective potent and non-toxic inhibitors stimulating basal ATPase activity, Drug Des., Dev. Ther., 9 (2015) 3481-3495.
[40] N.A. Gujarati, L. Zeng, P. Gupta, Z.-S. Chen, V.L. Korlipara, Design, synthesis and biological evaluation of benzamide and phenyltetrazole derivatives with amide and urea linkers as BCRP inhibitors, Bioorg. Med. Chem. Lett., 27 (2017) 4698-4704.
[41] M.K. Krapf, J. Gallus, V. Namasivayam, M. Wiese, 2,4,6-Substituted Quinazolines with Extraordinary Inhibitory Potency toward ABCG2, J. Med. Chem., 61 (2018) 7952-7976.
[42] A. Boumendjel, E. Nicolle, T. Moraux, B. Gerby, M. Blanc, X. Ronot, J. Boutonnat, Piperazinobenzopyranones and Phenalkylaminobenzopyranones: Potent Inhibitors of Breast Cancer Resistance Protein (ABCG2), J. Med. Chem., 48 (2005) 7275-7281.
[43] G. Valdameri, E. Genoux-Bastide, B. Peres, C. Gauthier, J. Guitton, R. Terreux, S.M.B. Winnischofer, M.E.M. Rocha, A. Boumendjel, A. Di Pietro, Substituted Chromones as Highly Potent Nontoxic Inhibitors, Specific for the Breast Cancer Resistance Protein, J. Med. Chem., 55 (2012) 966-970.
[44] A.d.R.A. Pires, F. Lecerf-Schmidt, N. Guragossian, J. Pazinato, G.J. Gozzi, E. Winter, G. Valdameri, A. Veale, A. Boumendjel, A. Di Pietro, B. Pérès, New, highly potent and non-toxic, chromone inhibitors of the human breast cancer resistance protein ABCG2, Eur. J. Med. Chem., 122 (2016) 291-301.
[45] S. Yang, K.-Y. Lee, R.-J. Chen, P. Lo, S.-Y. Liao, J.-D. Wu, C.-H.R. King, Preparation of 3-(quinolin-4-yl)-linked proline-containing peptidomimetics as HCV protease inhibitors, WO2008095058A1, 2008.
[46] A.L. Hopkins, C.R. Groom, A. Alex, Ligand efficiency: a useful metric for lead selection, Drug Discov. Today, 9 (2004) 430-431.
[47] J.D. Allen, A. Van Loevezijn, J.M. Lakhai, M. Van der Valk, O. Van Tellingen, G. Reid, J.H.M. Schellens, G.-J. Koomen, A.H. Schinkel, Potent and specific inhibition of the breast cancer resistance protein multidrug transporter in vitro and in mouse intestine by a novel analogue of fumitremorgin C, Mol. Cancer Ther., 1 (2002) 417-425.
[48] G. Luurtsema, P. Elsinga, R. Dierckx, R. Boellaard, A. van Waarde, PET Tracers for Imaging of ABC Transporters at the Blood-Brain Barrier: Principles and Strategies, Curr. Pharm. Des., 22 (2016) 5779-5785.
[49] C. Özvegy, T. Litman, G. Szakács, Z. Nagy, S. Bates, A. Váradi, B. Sarkadi, Functional Characterization of the Human Multidrug Transporter, ABCG2, Expressed in Insect Cells, Biochem. Biophys. Res. Commun., 285 (2001) 111-117.
[50] T. Litman, T.E. Druley, W.D. Stein, S.E. Bates, From MDR to MXR: new understanding of multidrug resistance systems, their properties and clinical significance, Cell. Mol. Life Sci., 58 (2001) 931-959.
[51] A. Gaspar, M.J. Matos, J. Garrido, E. Uriarte, F. Borges, Chromone: A Valid Scaffold in Medicinal Chemistry, Chem. Rev., 114 (2014) 4960-4992.
[52] J. Reis, A. Gaspar, N. Milhazes, F. Borges, Chromone as a Privileged Scaffold in Drug Discovery: Recent Advances, J. Med. Chem., 60 (2017) 7941-7957.

[53] M.A. Ibrahim, N.M. El-Gohary, S. Said, Ring opening ring closure reactions with 3-substituted chromones under nucleophilic conditions, Heterocycles, 91 (2015) 1863-1903.
[54] IUPAC, Compendium of Chemical Terminology http://goldbook.iupac.org/terms/view/S05740 (accessed February 24, 2020).
[55] H. Gamsjäger, J.W. Lorimer, P. Scharlin, D.G. Shaw, Glossary of terms related to solubility (IUPAC Recommendations 2008), Pure Appl. Chem., 80 (2008) 233.
[56] M. Apley, G.B. Crist, V. Fellner, M.A. Gonzalez, R.P. Hunter, M.N. Martinez, J.R. Messenheimer, S. Modric, M.G. Papich, A.F. Parr, J.E. Riviere, M.R.C. Marques, Determination of thermodynamic solubility of active pharmaceutical ingredients for veterinary species: a new USP general chapter, Dissolution Technol., 24 (2017) 36-39.
[57] C.D. Bevan, R.S. Lloyd, A High-Throughput Screening Method for the Determination of Aqueous Drug Solubility Using Laser Nephelometry in Microtiter Plates, Anal. Chem., 72 (2000) 1781-1787.
[58] B. Hoelke, S. Gieringer, M. Arlt, C. Saal, Comparison of Nephelometric, UV-Spectroscopic, and HPLC Methods for High-Throughput Determination of Aqueous Drug Solubility in Microtiter Plates, Anal. Chem., 81 (2009) 3165-3172.
[59] J. Alsenz, M. Kansy, High throughput solubility measurement in drug discovery and development, Adv. Drug Delivery Rev., 59 (2007) 546-567.
[60] C. Saal, A.C. Petereit, Optimizing solubility: Kinetic versus thermodynamic solubility temptations and risks, Eur. J. Pharm. Sci., 47 (2012) 589-595.
[61] D. Mackay, W.Y. Shiu, Aqueous solubility of polynuclear aromatic hydrocarbons, J. Chem. Eng. Data, 22 (1977) 399-402.
[62] M. Abedi, R. Ahangari Cohan, M. Shafiee Ardestani, F. Davami, Comparison of polystyrene versus cycloolefin microplates in absorbance measurements in the UV/VIS region of the spectrum, J. Shahrekord Univ. Med. Sci., 21 (2019) 110-113.
[63] J.P.L. Damasceno, C.d.S. Giuberti, R.d.C.R. Gonçalves, R.R. Kitagawa, Preformulation study and influence of DMSO and propylene glycol on the antioxidant action of isocoumarin paepalantine isolated from Paepalanthus bromelioides, Rev. Bras. Farmacogn., 25 (2015) 395-400.
[64] F. Cataldo, O. Ursini, G. Angelini, S. Iglesias-Groth, On the Way to Graphene: The Bottom-Up Approach to Very Large PAHs Using the Scholl Reaction, Fullerenes, Nanotubes, Carbon Nanostruct., 19 (2011) 713-725.
[65] E. Huber, M. Frost, Light scattering by small particles, J. Water Supply: Res. Technol. - Aqua, 47 (1998) 87-94.
[66] M.I. Jeraal, K.J. Roberts, I. McRobbie, D. Harbottle, Process-Focused Synthesis, Crystallization, and Physicochemical Characterization of Sodium Lauroyl Isethionate, ACS Sustainable Chem. Eng., 6 (2018) 2667-2675.
[67] Y.W. Alelyunas, R. Liu, L. Pelosi-Kilby, C. Shen, Application of a Dried-DMSO rapid throughput 24-h equilibrium solubility in advancing discovery candidates, Eur. J. Pharm. Sci., 37 (2009) 172-182.
[68] L. Zhou, L. Yang, S. Tilton, J. Wang, Development of a high throughput equilibrium solubility assay using miniaturized shake□flask method in early drug discovery, J. Pharm. Sci., 96 (2007) 3052-3071.
[69] E. Baka, J.E.A. Comer, K. Takács-Novák, Study of equilibrium solubility measurement by saturation shake-flask method using hydrochlorothiazide as model compound, J. Pharm. Biomed. Anal., 46 (2008) 335-341.
[70] NIH PubChem, Haloperidol: CID=3559, https://pubchem.ncbi.nlm.nih.gov/compound/Haloperidol (accessed February 24, 2020).
[71] K. Valkó, Application of high-performance liquid chromatography based measurements of lipophilicity to model biological distribution, J. Chromatogr. A, 1037 (2004) 299-310.

[72] N.M. Kershaw, G.S.A. Wright, R. Sharma, S.V. Antonyuk, R.W. Strange, N.G. Berry, P. M. O'Neill, S.S. Hasnain, X-ray Crystallography and Computational Docking for the Detection and Development of Protein–Ligand Interactions, Curr. Med. Chem., 20 (2013) 569-575.
[73] X. Guo, K.K.W. To, Z. Chen, X. Wang, J. Zhang, M. Luo, F. Wang, S. Yan, L. Fu, Dacomitinib potentiates the efficacy of conventional chemotherapeutic agents via inhibiting the drug efflux function of ABCG2 in vitro and in vivo, J. Exp. Clin. Cancer Res., 37 (2018) 31/31-31/13.
[74] M. Hubensack, C. Mueller, P. Hoecherl, S. Fellner, T. Spruss, G. Bernhardt, A. Buschauer, Effect of the ABCB1 modulators elacridar and tariquidar on the distribution of paclitaxel in nude mice, J. Cancer Res. Clin. Oncol., 134 (2008) 597-607.
[75] E.M. Leslie, R.G. Deeley, S.P.C. Cole, Multidrug resistance proteins: role of P-glycoprotein, MRP1, MRP2, and BCRP (ABCG2) in tissue defense, Toxicol. Appl. Pharmacol., 204 (2005) 216-237.
[76] M.A. Martí-Renom, A.C. Stuart, A. Fiser, R. Sánchez, F. Melo, A. Šali, Comparative Protein Structure Modeling of Genes and Genomes, Annu. Rev. Biophys. Biomol. Struct., 29 (2000) 291-325.
[77] A. Šali, T.L. Blundell, Comparative Protein Modelling by Satisfaction of Spatial Restraints, J. Mol. Biol., 234 (1993) 779-815.
[78] A. Fiser, R.K.G. Do, A. Šali, Modeling of loops in protein structures, Protein Sci., 9 (2000) 1753-1773.
[79] A. Pegoli, X. She, D. Wifling, H. Hübner, G. Bernhardt, P. Gmeiner, M. Keller, Radiolabeled Dibenzodiazepinone-Type Antagonists Give Evidence of Dualsteric Binding at the M2 Muscarinic Acetylcholine Receptor, J. Med. Chem., 60 (2017) 3314-3334.
[80] A. Pegoli, D. Wifling, C.G. Gruber, X. She, H. Hübner, G. Bernhardt, P. Gmeiner, M. Keller, Conjugation of Short Peptides to Dibenzodiazepinone-Type Muscarinic Acetylcholine Receptor Ligands Determines M2R Selectivity, J. Med. Chem., 62 (2019) 5358-5369.
[81] S. Salentin, S. Schreiber, V.J. Haupt, M.F. Adasme, M. Schroeder, PLIP: fully automated protein-ligand interaction profiler, Nucleic Acids Res., 43 (2015) W443-W447.
[82] M. Roe, A. Folkes, P. Ashworth, J. Brumwell, L. Chima, S. Hunjan, I. Pretswell, W. Dangerfield, H. Ryder, P. Charlton, Reversal of P-glycoprotein mediated multidrug resistance by novel anthranilamide derivatives, Bioorg. Med. Chem. Lett., 9 (1999) 595-600.
[83] M. Hubensack, Approaches to Overcome the Blood-Brain Barrier in the Chemotherapy of Primary and Secondary Brain Tumors: Modulation of P-glycoprotein 170 and Targeting of the Transferrin Receptor, Dissertation, University of Regensburg, 2005, https://epub.uni-regensburg.de/10297/.
[84] C.-H. Yang, E. Schneider, M.-L. Kuo, E.L. Volk, E. Rocchi, Y.-C. Chen, BCRP/MXR/ABCP expression in topotecan-resistant human breast carcinoma cells, Biochem. Pharmacol., 60 (2000) 831-837.
[85] M. Kühnle, M. Egger, C. Müller, A. Mahringer, G. Bernhardt, G. Fricker, B. König, A. Buschauer, Potent and Selective Inhibitors of Breast Cancer Resistance Protein (ABCG2) Derived from the p-Glycoprotein (ABCB1) Modulator Tariquidar, J. Med. Chem., 52 (2009) 1190-1197.
[86] K. Kohno, J. Kikuchi, S. Sato, H. Takano, Y. Saburi, K. Asoh, M. Kuwano, Vincristine-resistant human cancer KB cell line and increased expression of multidrug-resistance gene, Jpn. J. Cancer Res., 79 (1988) 1238-1246.
[87] R. Evers, M. Kool, L. van Deemter, H. Janssen, J. Calafat, L.C. Oomen, C.C. Paulusma, R.P. Oude Elferink, F. Baas, A.H. Schinkel, P. Borst, Drug export activity of the human canalicular multispecific organic anion transporter in polarized kidney MDCK cells expressing cMOAT (MRP2) cDNA, J. Clin. Invest., 101 (1998) 1310-1319.

[88] E. Bakos, R. Evers, G. Szakacs, G.E. Tusnady, E. Welker, K. Szabo, M. De Haas, L. Van Deemter, P. Borst, A. Varadi, B. Sarkadi, Functional multidrug resistance protein (MRP1) lacking the N-terminal transmembrane domain, J. Biol. Chem., 273 (1998) 32167-32175.
[89] B. Sarkadi, E.M. Price, R.C. Boucher, U.A. Germann, G.A. Scarborough, Expression of the human multidrug resistance cDNA in insect cells generates a high activity drug-stimulated membrane ATPase, J. Biol. Chem., 267 (1992) 4854-4858.

Highlights

Water-Soluble Inhibitors of ABCG2 (BCRP) – A Fragment-Based and Computational Approach

Frauke Antoni*, David Wifling, Günther Bernhardt

Institute of Pharmacy, University of Regensburg, D-93040 Regensburg, Germany

- We discovered water-soluble ABCG2 inhibitors by a fragment-based approach
- Molecular docking studies were included to optimize the inhibitors
- Multiplication of solubility was achieved while maintaining inhibitory potency
- The series contains ABCG2-selective as well as triple ABCB1/C1/G2 inhibitors
- They were stable in blood plasma and non-toxic

Declaration of interests

☒ The authors declare that they have no known competing financial interests or personal relationships that could have appeared to influence the work reported in this paper.

☐The authors declare the following financial interests/personal relationships which may be considered as potential competing interests: